Computer Assisted Methods in Engineering and Science, **22**: 177–204, 2015.

Discontinuous Galerkin method on reference domain

Jan Jaśkowiec
Cracow University of Technology, Faculty of Civil Engineering
Institute for Computational Civil Engineering
Warszawska 24, 31-155 Cracow, Poland
e-mail: j.jaskowiec@L5.pk.edu.pl

A reference domain is chosen to formulate numerical model using the discontinuous Galerkin with finite difference (DGFD) method. The differential problem, which is defined for the real domain, is transformed in a weak form to the reference domain. The shape of the real domain results from a considered problem which can be complex. On the other hand, a reference domain can be chosen to be, for example, cube or square, which is convenient for meshing and calculations. Transformation from the reference domain into the real one has to be defined. In this paper, the algorithm for such a transformation is proposed, which is based on second-order differential equations. The paper presents a series of benchmark examples that show both the correctness and flexibility of the proposed algorithms. In the majority of the examples, the reference domain is square when the real domains are, for example, quarter of annulus, circle or full annulus.

Keywords: discontinuous Galerkin method, domain transformation, reference domain.

1. Introduction

This paper concerns the discontinuous Galerkin (DG) method in which all the calculations are performed not on a problem domain, but a reference domain. It means that in the approach presented in this work two domains are considered: the real domain in which the problem is defined and the reference domain in which the discretization and DG method are carried out. The real domain V comes from the problem definition and very often its shape is quite complicated and thus problematic to discretize and to obtain good approximate solution. In standard approach, the finite element (FE) mesh is constructed on the real domain. In that case, with the real domain having curved boundaries, the FE mesh has to adjusted to the boundary so that the domain geometry is represented by the mesh accurate as possible. The strict domain reconstructing using an FE mesh is not always possible even when high-order finite elements are used. In such cases, the domain is only approximated by the mesh.

In the standard finite element (FE) or standard DG methods, the considered domain is discretized by finite elements. Integrations over each finite element are calculated for the reference finite element and the results are transformed back to the real finite element. In consequence, the algebraic system of equations is defined on the mesh constructed for the real domain. It is important for the mesh that each element cell is well defined, i.e., a cell is not elongated, and it does not have very acute or too obtuse angles. In some situations, it is hard to meet these requirements due to a complex domain shape or in the case of analysis of large deformations due to the mesh being deformed within the domain. Mesh distortions can be handled by the arbitrary Lagrangian-Eulerian (ALE) descriptions [5–7, 9, 20]. However, the ALE analysis produces some complications since the domain and the mesh deformations are analyzed separately.

In the proposed approach the reference domain is introduced on which all the calculations are performed. The shape of the reference domain is at user, choice, and usually it has nothing to

do with the real domain. The shape of the reference domain should be as simple as possible to ensure easy mesh generation. For example, in case of three-dimensional problem the reference domain can be cubic or parallelepiped. In two-dimensional case, the reference domain should be square or rectangular. The results of calculations are obtained for the reference domain and the transformation to the real domain is therefore necessary.

In this paper, it is proposed how to generate a transformation from a reference domain to a real domain. The method for generating this transformation is based on a set of second-order partial differential equations defined on the reference domain with Dirichlet boundary conditions on the outer boundary. In this approach, the boundary conditions come from the position of points that belong to the outer boundary in the real domain. Then, the differential equations are transformed into weak forms and solved using a set of basis functions. The basis functions can be, for example, high-degree polynomials or other functions if necessary. For instance, the trigonometrical basis functions are used in some examples presented in this paper. The presented equations are formulated for three-dimensional domains. However, the examples in this paper refer to two-dimensional cases. In this work, among others things it is shown how to transform a square domain into circle, quarter of annulus or L-shaped domains. In some cases, the choice of reference domain has to take into account the shape of the real domain. For example, the square reference domain with a square hole inside is transformed into a circular annulus.

The discontinuous Galerkin (DG) method is chosen as a computational method to find approximate solution in the reference domain. However, other methods can be used, such as the finite element method or one of the meshless methods. For the reference domain, the polygonal mesh is used, and for such a mesh the DG method, in which a high-ordered approximation can be applied, is appropriate. The DG method was developed in the early 1970s [18] and since then it has been constantly refined/evolving, see, e.g., [2, 4, 8, 19]. The type of DG method called the DG finite difference (DGFD) method presented in [11] is applied in this paper. In the examples, the polygonal finite element meshes are used [11]. For the sake of clarity, the scalar elliptic problem is considered in order to present the approach. However, it can be directly extended to other kinds of problems. A typical example of the scalar elliptic problem is a problem involving heat transfer Fourier's law.

The proposed approach is quite similar to analysis involving large deformations [13–15, 17, 20]. However, in the presented method the shape of the reference domain is at user's choice. The DGFD method requires the finite difference (FD) rules for compatibility conditions between the neighboring elements and to satisfy the Dirichlet boundary conditions. A special attention has to be paid to the FD rules on the reference domain since the transformation from the real into the reference domain has to be taken into account. A detailed description of the algorithm is described in the subsequent sections.

On the other hand, some similarities with the isogeometric analysis (IGA) can be noticed. In the IGA, the shape functions are constructed on the basis of NURBS and a set of control points. In effect, almost the exact geometry representation can be obtained [1, 3, 10]. In this work, the DGFD method also deals with exact geometry representation. However, in contrary to the IGA, no complicated shape functions or control points are needed. The geometry representation is constructed by using a set of basis functions which can consist of high-degree polynomials or some special functions.

The methodology presented in this work can be summarized as follows: i) the elliptic problem is defined on the real domain, ii) the shape of the reference domain is chosen, iii) the transformation from the reference domain into real one is generated, iv) the polygonal finite element mesh is generated on the reference domain, v) the approximate solution on the reference domain is obtained using the DGFD method, vi) the approximate solution is transformed into the real domain.

In section, the DGFD method is derived on the reference domain. Subsequently, in Sec. 3 the approximation technique is described. Section 4 presents the details connected with transformation from the reference into the real domain. The DGFD method used on the reference domain is illustrated with a series of examples which are discussed in Sec. 5. Finally, in last, Sec. 6, some conclusions are presented.

2. DGFD method on reference domain

The domain V with outer boundary S is considered. For the sake of clarity, the domain is referred to, in this paper, as the real domain. The following, boundary problem that can be understood as a conductivity heat transport problem is formulated for this domain:

$$\begin{aligned} &\operatorname{div}\mathbf{q} - r = 0, && \text{on} \quad V,\\ &\mathbf{q} = -\lambda\nabla\Theta, && \text{on} \quad V,\\ &\Theta = \widehat{\Theta}, && \text{on} \quad S_\Theta,\\ &\mathbf{q}\cdot\mathbf{n} = \widehat{h}, && \text{on} \quad S_q, \end{aligned} \tag{1}$$

where Θ is the temperature, $\mathbf{q}$ is the heat flux vector, r the heat source density, λ is the heat conductivity parameter for a thermally isotropic material, $\widehat{\Theta}$ and $\widehat{h}$ are prescribed values of temperature and heat flux, respectively, S_Θ is the part of S where the temperature $\widehat{\Theta}$ is prescribed, S_q is the part of S where the heat flux $\widehat{h}$ is prescribed, and $\mathbf{n}$ is the unit vector normal to the outer boundary. The heat flux vector is related to the temperature field by using Fourier's law included in $(1)_2$.

The formulation of the DGFD method starts with the weak form of the analyzed problem (1), with the test function v

$$\int_V v\operatorname{div}\mathbf{q}\,\mathrm{d}V - \int_V vr\,\mathrm{d}V = 0, \qquad \forall\, v. \tag{2}$$

The considered problem is going to be solved on finite element mesh, in which the approximations on finite elements are not continuous when going from one element to another. Thus, the mesh skeleton S_s need to be distinguished in the mesh that is defined as the inter-element border. In consequence, the approximation field is not continuous on S_s. The discontinuity of mesh skeleton needs to be taken into account in the subsequent analysis. When integration by parts is performed on the first component from Eq. (2), it results in

$$\int_{S_q} v\mathbf{q}\cdot\mathbf{n}\,\mathrm{d}S + \int_{S_\Theta} v\mathbf{q}\cdot\mathbf{n}\,\mathrm{d}S - \int_V \nabla v\cdot\mathbf{q}\,\mathrm{d}V + \int_{S_s} [\![v\mathbf{q}]\!]\cdot\mathbf{n}\,\mathrm{d}S - \int_V vr\,\mathrm{d}V = 0, \tag{3}$$

in which the fourth integral appears due to the discontinuity on S_s.

The definitions of the jump and mid-value operators $[\![\bullet]\!]$, $\langle\bullet\rangle$ on S_s are defined in this work as follows:

$$[\![f]\!] = \lim_{\epsilon\to 0}[\![f]\!]_\epsilon, \qquad \langle f\rangle(\mathbf{x}) = \lim_{\epsilon\to 0}\langle f\rangle_\epsilon, \tag{4}$$

where the jump and mean values at distance ϵ are defined as follows:

$$[\![f]\!]_\epsilon = f(\mathbf{x}+\epsilon\,\mathbf{n}) - f(\mathbf{x}-\epsilon\,\mathbf{n}), \qquad \langle f\rangle_\epsilon = 0.5\,(f(\mathbf{x}+\epsilon\,\mathbf{n}) + f(\mathbf{x}-\epsilon\,\mathbf{n})). \tag{5}$$

It is a well-known property that a jump of two functions' superposition can be expressed as follows:

$$[\![fg]\!] = [\![f]\!]\,\langle g\rangle + \langle f\rangle\,[\![g]\!]. \tag{6}$$

The domain V represents the real configuration domain described in global coordinates $\mathbf{x}$. It may happen that the domain V has a quite complicated shape so that the finite element discretization can be quite complicated and finite element mesh can not represent its geometry exactly. It is possible to 'shift' the calculation to the other, so-called, reference domain Ω whose shape can be,

for example, cubic (in 3D) or square (in 2D). In the Ω domain, the discretization and further calculations can be performed in a quite easy way. The results of these calculation can be then transformed back to the V domain. In the reference domain, the other coordinate system $\boldsymbol{\xi}$ is used. The transformation between these two coordinate systems can be derived, i.e., $\mathbf{x} = \mathbf{x}(\boldsymbol{\xi})$ and the reverse is $\boldsymbol{\xi} = \boldsymbol{\xi}(\mathbf{x})$, see Fig. 1. The coordinates' vectors $\mathbf{x}$ and $\boldsymbol{\xi}$ are defined in three-dimensional spaces

$$\mathbf{x} = \begin{bmatrix} x \\ y \\ z \end{bmatrix}, \qquad \boldsymbol{\xi} = \begin{bmatrix} \xi \\ \eta \\ \theta \end{bmatrix}. \tag{7}$$

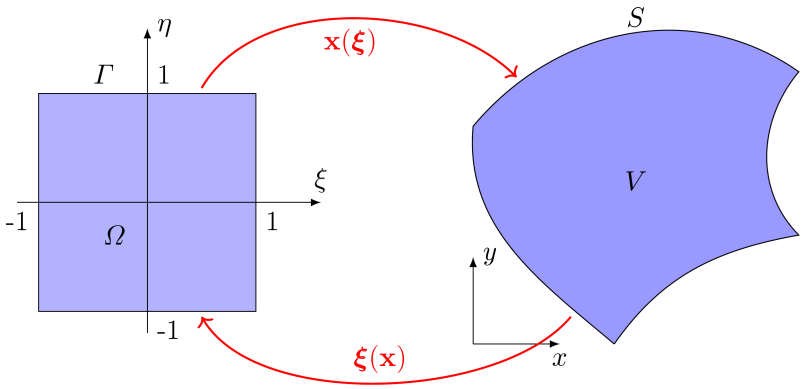

Fig. 1. Transformation from the reference domain Ω to the real domain V.

The infinitely small increments are transformed between the domains by the so-called transformation tensors $\mathbf{F}$ and $\mathbf{G}$

$$\mathrm{d}\mathbf{x} = \mathbf{F}\,\mathrm{d}\boldsymbol{\xi}, \qquad \mathrm{d}\boldsymbol{\xi} = \mathbf{G}\,\mathrm{d}\mathbf{x}, \tag{8}$$

where

$$\mathbf{F} = \frac{\partial \mathbf{x}}{\partial \boldsymbol{\xi}} = \begin{bmatrix} \dfrac{\partial x}{\partial \xi} & \dfrac{\partial x}{\partial \eta} & \dfrac{\partial x}{\partial \theta} \\ \dfrac{\partial y}{\partial \xi} & \dfrac{\partial y}{\partial \eta} & \dfrac{\partial y}{\partial \theta} \\ \dfrac{\partial z}{\partial \xi} & \dfrac{\partial z}{\partial \eta} & \dfrac{\partial z}{\partial \theta} \end{bmatrix}, \qquad \mathbf{G} = \frac{\partial \boldsymbol{\xi}}{\partial \mathbf{x}} = \begin{bmatrix} \dfrac{\partial \xi}{\partial x} & \dfrac{\partial \xi}{\partial y} & \dfrac{\partial \xi}{\partial z} \\ \dfrac{\partial \eta}{\partial x} & \dfrac{\partial \eta}{\partial y} & \dfrac{\partial \eta}{\partial z} \\ \dfrac{\partial \theta}{\partial x} & \dfrac{\partial \theta}{\partial y} & \dfrac{\partial \theta}{\partial z} \end{bmatrix}. \tag{9}$$

The determinants of these tensors are called the Jacobians of the transformations

$$J_F = \det(\mathbf{F}), \qquad J_G = \det(\mathbf{G}). \tag{10}$$

It can be easily noticed that

$$\mathbf{F}^{-1} = \mathbf{G}, \qquad \frac{1}{J_F} = J_G. \tag{11}$$

The transformation tensors can be used to transform gradients between these two coordinates. Let us assume that there is a function a defined for V and the adequate function for Ω is A so that

$$a(\mathbf{x}) = a\left(\mathbf{x}(\boldsymbol{\xi})\right) = A\left(\boldsymbol{\xi}\right). \tag{12}$$

In this paper of the convention is adapted from the analysis of large deformations in which the functions in the real domain are denoted by small letters and the corresponding functions in the reference domain are written in capital letters.

The relationships between gradients of a and A in $\mathbf{x}$ and $\boldsymbol{\xi}$ coordinates, respectively, are as follows:

$$\nabla_{\mathbf{x}} a\left(\mathbf{x}(\boldsymbol{\xi})\right) = \begin{bmatrix} \dfrac{\partial a}{\partial x} \\ \dfrac{\partial a}{\partial y} \\ \dfrac{\partial a}{\partial z} \end{bmatrix} = \begin{bmatrix} \dfrac{\partial a}{\partial \xi}\dfrac{\partial \xi}{\partial x} + \dfrac{\partial a}{\partial \eta}\dfrac{\partial \eta}{\partial x} + \dfrac{\partial a}{\partial \theta}\dfrac{\partial \theta}{\partial x} \\ \dfrac{\partial a}{\partial \xi}\dfrac{\partial \xi}{\partial y} + \dfrac{\partial a}{\partial \eta}\dfrac{\partial \eta}{\partial y} + \dfrac{\partial a}{\partial \theta}\dfrac{\partial \theta}{\partial y} \\ \dfrac{\partial a}{\partial \xi}\dfrac{\partial \xi}{\partial z} + \dfrac{\partial a}{\partial \eta}\dfrac{\partial \eta}{\partial z} + \dfrac{\partial a}{\partial \theta}\dfrac{\partial \theta}{\partial z} \end{bmatrix}$$

$$= \begin{bmatrix} \dfrac{\partial \xi}{\partial x} & \dfrac{\partial \eta}{\partial x} & \dfrac{\partial \theta}{\partial x} \\ \dfrac{\partial \xi}{\partial y} & \dfrac{\partial \eta}{\partial y} & \dfrac{\partial \theta}{\partial y} \\ \dfrac{\partial \xi}{\partial z} & \dfrac{\partial \eta}{\partial z} & \dfrac{\partial \theta}{\partial z} \end{bmatrix} \begin{bmatrix} \dfrac{\partial a}{\partial \xi} \\ \dfrac{\partial a}{\partial \eta} \\ \dfrac{\partial a}{\partial \theta} \end{bmatrix} = \mathbf{G}^{\mathrm{T}} \nabla_{\boldsymbol{\xi}} a\left(\mathbf{x}(\boldsymbol{\xi})\right) = \mathbf{G}^{\mathrm{T}} \nabla_{\boldsymbol{\xi}} A\left(\boldsymbol{\xi}\right), \quad (13)$$

where $\nabla_{\mathbf{x}}$ and $\nabla_{\boldsymbol{\xi}}$ are the gradient operators in the $\mathbf{x}$ and $\boldsymbol{\xi}$ coordinates, respectively.

Five integrals in Eq. (3) are written in the real configuration V. However, they can be rewritten in the reference configuration Ω, which is presented below successively for each of the integrals.

The fifth integral in Eq. (3) is over the whole real domain and its transformation to the reference domain is direct since there are no differential operators

$$I_5 = \int_V vr \,\mathrm{d}V = \int_V v(\mathbf{x}) r(\mathbf{x}) \,\mathrm{d}V = \int_\Omega v\left(\mathbf{x}(\boldsymbol{\xi})\right) r\left(\mathbf{x}(\boldsymbol{\xi})\right) J_F\left(\boldsymbol{\xi}\right) \mathrm{d}\Omega$$

$$= \int_\Omega V\left(\boldsymbol{\xi}\right) R\left(\boldsymbol{\xi}\right) J_F\left(\boldsymbol{\xi}\right) \mathrm{d}\Omega = \int_\Omega VRJ_F \mathrm{d}\Omega. \quad (14)$$

The third integral is also over V but its transformation to the reference domain is more complicated due to gradients in the integrand. In this case, the relationship from Eq. (13) has to be taken into account

$$I_3 = \int_V \nabla v \cdot \mathbf{q} \,\mathrm{d}V = \int_V \left(\nabla v\right)^{\mathrm{T}} \mathbf{q} \,\mathrm{d}V = \int_V \left(\nabla_{\mathbf{x}} v(\mathbf{x})\right)^{\mathrm{T}} \mathbf{q}(\mathbf{x}) \,\mathrm{d}V$$

$$= \int_\Omega \left(\nabla_{\mathbf{x}} v\left(\mathbf{x}(\boldsymbol{\xi})\right)\right)^{\mathrm{T}} \mathbf{q}\left(\mathbf{x}(\boldsymbol{\xi})\right) J_F\left(\boldsymbol{\xi}\right) \,\mathrm{d}\Omega = \int_\Omega \left(\nabla_{\boldsymbol{\xi}} V\right)^{\mathrm{T}} \mathbf{G}\,\mathbf{q}\, J_F \,\mathrm{d}\Omega = \int_\Omega \left(\nabla_{\boldsymbol{\xi}} V\right)^{\mathrm{T}} \mathbf{Q} \,\mathrm{d}\Omega, \quad (15)$$

where $\mathbf{Q} = J_F \mathbf{G}\mathbf{q}$ is the heat flux vector in the reference domain. The heat flux on the V domain is related to temperature gradient by the Fourier's law, i.e., $(1)_2$. In the reference domain, Fourier's law has the following form:

$$\mathbf{Q} = J_F \mathbf{G}\mathbf{q} = J_F \mathbf{G}\left(-\lambda \nabla_{\mathbf{x}} \Theta\right) = -\lambda J_F \mathbf{G}\mathbf{G}^{\mathrm{T}} \nabla_{\boldsymbol{\xi}} \Theta = -\boldsymbol{\Lambda} \nabla_{\boldsymbol{\xi}} \Theta, \quad (16)$$

where $\boldsymbol{\Lambda} = \lambda J_F \mathbf{G}\mathbf{G}^{\mathrm{T}}$ is the conductivity matrix in the reference domain. Now, the integral I_3 holds as

$$I_3 = -\int_\Omega \left(\nabla_{\boldsymbol{\xi}} V\right)^{\mathrm{T}} \boldsymbol{\Lambda} \nabla_{\boldsymbol{\xi}} \Theta \,\mathrm{d}\Omega. \quad (17)$$

The first integral I_1 in Eq. (3) is over S_q where the outer heat flux $\widehat{h}$ is prescribed. The integral is over a surface thus the transformation to the reference configuration requires a transformation Jacobian based on the Nanson's formula [16], which describes the relationship of infinitesimally small areas in the real and reference configurations

$$J_F^n(\mathbf{n}) = J_F \|\mathbf{G}^{\mathrm{T}}\mathbf{n}\| = \frac{\mathrm{d}S}{\mathrm{d}\Gamma}. \tag{18}$$

The transformation of I_1 from real to reference configuration is then as follows:

$$\begin{aligned} I_1 = \int_{S_q} v\mathbf{q}\cdot\mathbf{n}\,\mathrm{d}S = \int_{S_q} v\,\widehat{h}\,\mathrm{d}S = \int_{S_q} v(\mathbf{x})\widehat{h}(\mathbf{x})\,\mathrm{d}S = \int_{\Gamma_q} v\left(\mathbf{x}(\boldsymbol{\xi})\right)\widehat{h}\left(\mathbf{x}(\boldsymbol{\xi})\right) J_F^n(\mathbf{n})\,\mathrm{d}\Gamma \\ = \int_{\Gamma_q} V\left(\boldsymbol{\xi}\right)\widehat{H}\left(\boldsymbol{\xi}\right) J_F^n(\mathbf{n})\,\mathrm{d}\Gamma = \int_{\Gamma_q} V\widehat{H} J_F^n(\mathbf{n})\,\mathrm{d}\Gamma. \end{aligned} \tag{19}$$

The second integral I_2 in Eq. (3) is calculated over the part of the outer surface where the Dirichlet conditions are defined. If the standard shape functions were used the Dirichlet conditions could be applied directly to the degrees of freedom on the nodes belonging to the boundary. However, in this work the DGFD method is used, in which there are no nodes or shape functions. In the DGFD method, essential boundary conditions are defined with the help of a fourth-degree finite difference rule. The Dirichlet boundary conditions are applied directly to the reference configuration. That is why, in the reference configuration, the integral I_2 does not have a Jacobian transformation. After these clarifications, the integral can be expressed as

$$I_2 = \int_{S_\Theta} v\mathbf{q}\cdot\mathbf{n}\,\mathrm{d}S = \int_{S_\Theta} vh\,\mathrm{d}S = \int_{\Gamma_\Theta} VH\,\mathrm{d}\Gamma. \tag{20}$$

The heat flux H on Γ_Θ is equivalent to the heat flux vector in the reference domain $\mathbf{Q}$, defined in Eq. (16), projected normal to the boundary in the reference domain, i.e.,

$$H = \mathbf{Q}\cdot\mathbf{N} = -\boldsymbol{\Lambda}\nabla_{\boldsymbol{\xi}}\Theta\cdot\mathbf{N} = -\mathbf{N}^{\mathrm{T}}\boldsymbol{\Lambda}\nabla_{\boldsymbol{\xi}}\Theta. \tag{21}$$

Every vector in the reference coordinates $\boldsymbol{\xi}$ can be expressed by the coefficients in the boundary local coordinates which are defined by a set of mutually perpendicular unit vectors ($\mathbf{N}$, $\mathbf{S}$, $\mathbf{R}$):

$$\mathbf{V} = \begin{bmatrix} V_\xi \\ V_\eta \\ V_\theta \end{bmatrix} = \mathbf{N}V_N + \mathbf{S}V_S + \mathbf{R}V_R = \mathbf{T}\begin{bmatrix} V_N \\ V_S \\ V_R \end{bmatrix} = \mathbf{T}\mathbf{V}^{\mathbf{N}}, \tag{22}$$

where V_ξ, V_η and V_θ are the vector coefficients in the $\boldsymbol{\xi}$ coordinates, V_N, V_S and V_R are the vector coefficients in the boundary local coordinates. The matrix $\mathbf{T} = \begin{bmatrix} \mathbf{N} & \mathbf{S} & \mathbf{R} \end{bmatrix}$ is the transformation matrix in the reference domain that is used for transformation from the boundary local coordinates to the global ones.

It can be easily noticed that

$$\mathbf{N} = \mathbf{T}\begin{bmatrix} 1 \\ 0 \\ 0 \end{bmatrix} \tag{23}$$

and

$$\nabla_{\boldsymbol{\xi}}\Theta = \mathbf{T}\begin{bmatrix}\dfrac{\partial\Theta}{\partial N}\\[2ex] \dfrac{\partial\Theta}{\partial S}\\[2ex] \dfrac{\partial\Theta}{\partial R}\end{bmatrix} = \mathbf{T}\nabla_{\mathbf{N}}\Theta, \tag{24}$$

where $\dfrac{\partial\Theta}{\partial N}$, $\dfrac{\partial\Theta}{\partial S}$ and $\dfrac{\partial\Theta}{\partial R}$ are the partial derivatives in the directions defined by the unit vectors $\mathbf{N}$, $\mathbf{S}$ and $\mathbf{R}$, respectively and $\nabla_{\mathbf{N}}$ denotes the gradient operator in the boundary local coordinates.

Equations (23) and (24) can now be substituted into Eq. (21). The boundary heat flux is then

$$\begin{aligned} H &= -\begin{bmatrix}1 & 0 & 0\end{bmatrix}\mathbf{T}^{\mathrm{T}}\boldsymbol{\Lambda}\mathbf{T}\nabla_{\mathbf{N}^s}\Theta = -\begin{bmatrix}1 & 0 & 0\end{bmatrix}\boldsymbol{\Lambda}^{\mathbf{N}}\nabla_{\mathbf{N}^s}\Theta \\ &= -\left(\boldsymbol{\Lambda}^{\mathbf{N}}\right)_{11}\frac{\partial\Theta}{\partial N} - \left(\boldsymbol{\Lambda}^{\mathbf{N}}\right)_{12}\frac{\partial\Theta}{\partial S} - \left(\boldsymbol{\Lambda}^{\mathbf{N}}\right)_{13}\frac{\partial\Theta}{\partial R}, \qquad \text{on } S_\Theta, \end{aligned} \tag{25}$$

where $\boldsymbol{\Lambda}^{\mathbf{N}}$ is conductivity matrix in local boundary coordinates in the reference domain.

In order to apply the Dirichlet boundary conditions on Γ_Θ the derivative in the boundary normal direction is expressed by the fourth-degree finite difference rule [11]:

$$\frac{\partial\Theta}{\partial N} = 6\cdot\frac{\widehat{\Theta} - \Theta(\boldsymbol{\xi}_{2d})}{2d} - 4\overline{\nabla}_{\mathbf{N}}\Theta(\boldsymbol{\xi}_d) - \overline{\nabla}_{\mathbf{N}}\Theta(\boldsymbol{\xi}_{2d}), \qquad \text{on } \Gamma_\Theta, \tag{26}$$

where d is a scalar value that is small in relation to the characteristic size of finite elements, $\Theta(\boldsymbol{\xi}_d) = \boldsymbol{\xi} - d\mathbf{N}$, $\Theta(\boldsymbol{\xi}_2 d) = \boldsymbol{\xi} - 2d\mathbf{N}$, $\overline{\nabla}_{\mathbf{N}} = \nabla_{\boldsymbol{\xi}}\cdot\mathbf{N}$. The derivatives in $\mathbf{S}$ and $\mathbf{R}$ directions can be expressed by the gradients in the global coordinates:

$$\frac{\partial\Theta}{\partial S} = \nabla_{\boldsymbol{\xi}}\Theta\cdot\mathbf{S}, \qquad \frac{\partial\Theta}{\partial R} = \nabla_{\boldsymbol{\xi}}\Theta\cdot\mathbf{R}. \tag{27}$$

When Eqs. (25) to (27) are taken into account, the integral I_2 changes to the following form:

$$\begin{aligned} I_2 = &-\int_{\Gamma_\Theta} V\left(\boldsymbol{\Lambda}^{\mathbf{N}}\right)_{11}\left(6\cdot\frac{\widehat{\Theta} - \Theta(\boldsymbol{\xi}_{2d})}{2d} - 4\overline{\nabla}_{\mathbf{N}}\Theta(\boldsymbol{\xi}_d) - \overline{\nabla}_{\mathbf{N}}\Theta(\boldsymbol{\xi}_{2d})\right)\mathrm{d}\Gamma \\ &-\int_{\Gamma_\Theta} V\left(\left(\boldsymbol{\Lambda}^{\mathbf{N}}\right)_{12}\nabla_{\boldsymbol{\xi}}\Theta\cdot\mathbf{S} + \left(\boldsymbol{\Lambda}^{\mathbf{N}}\right)_{13}\nabla_{\boldsymbol{\xi}}\Theta\cdot\mathbf{R}\right)\mathrm{d}\Gamma. \end{aligned} \tag{28}$$

The fourth integral in Eq. (3) I_4 is defined over the mesh skeleton S_s. On the basis of [11] it is known that

$$[\![\mathbf{q}]\!]\cdot\mathbf{n} = 0. \tag{29}$$

Then, the integral I_4 is expressed as

$$I_4 = \int_{S_s}[\![v\mathbf{q}]\!]\cdot\mathbf{n}^s\,\mathrm{d}S = \int_{S_s}[\![v]\!]\,\mathbf{q}\cdot\mathbf{n}^s\,\mathrm{d}S = \int_{S_s}[\![v]\!]\,h_s\,\mathrm{d}S, \tag{30}$$

where h_s is the heat flux that 'goes' through the mesh skeleton.

The integral I_4 has to be rewritten also in the reference configuration. In such a case, the heat flux that goes' through the skeleton in the reference domain S_s is written directly in the reference configuration on the basis of Fourier's law in Eq. (21). Therefore, the integral I_4 can be rewritten as

$$I_4 = \int_{\Gamma_s} [\![V]\!] H_s \, \mathrm{d}\Gamma. \tag{31}$$

The skeleton heat flux can be stated in the same way as shown in Eq. (25), but now it is expressed in the skeleton local coordinates, i.e.,

$$H_s = -\left(\mathbf{\Lambda}^{\mathbf{N}}\right)_{11} \frac{\partial \Theta}{\partial N} - \left(\mathbf{\Lambda}^{\mathbf{N}}\right)_{12} \frac{\partial \Theta}{\partial S} - \left(\mathbf{\Lambda}^{\mathbf{N}}\right)_{13} \frac{\partial \Theta}{\partial R} \qquad \text{on } \Gamma_s. \tag{32}$$

The derivatives in the $\mathbf{S}$ and $\mathbf{R}$ directions are now computed using the mid-value operator

$$\frac{\partial \Theta}{\partial S} = \left\langle \nabla_{\boldsymbol{\xi}} \Theta \right\rangle \cdot \mathbf{S}, \qquad \frac{\partial \Theta}{\partial R} = \left\langle \nabla_{\boldsymbol{\xi}} \Theta \right\rangle \cdot \mathbf{R} \qquad \text{on } \Gamma_s. \tag{33}$$

The fourth-degree finite difference rule is applied to calculate the derivative in the normal direction [11]:

$$\frac{\partial \Theta}{\partial N} = \frac{3}{2} \cdot \frac{[\![\Theta]\!]_d}{2d} - \frac{1}{2} \cdot \left\langle \nabla_{\boldsymbol{\xi}} \Theta \right\rangle_d \cdot \mathbf{N}, \qquad \text{on } \Gamma_s. \tag{34}$$

After taking into account Eqs. (32) to (34) the integral I_4 changes to

$$I_4 = -\int_{\Gamma_s} [\![V]\!] \left(\mathbf{\Lambda}^{\mathbf{N}}\right)_{11} \left(\frac{3}{2} \cdot \frac{[\![\Theta]\!]_d}{2d} - \frac{1}{2} \cdot \left\langle \nabla_{\boldsymbol{\xi}} \Theta \right\rangle_d \cdot \mathbf{N} \right) \mathrm{d}\Gamma$$
$$- \int_{\Gamma_s} [\![V]\!] \left(\left(\mathbf{\Lambda}^{\mathbf{N}}\right)_{12} \left\langle \nabla_{\boldsymbol{\xi}} \right\rangle \Theta \cdot \mathbf{S} + \left(\mathbf{\Lambda}^{\mathbf{N}}\right)_{13} \left\langle \nabla_{\boldsymbol{\xi}} \right\rangle \Theta \cdot \mathbf{R} \right) \mathrm{d}\Gamma. \tag{35}$$

Finally, Eq. (3) has the following form

$$\int_{\Gamma_q} V \widehat{H} J_F^n(\mathbf{n}) \, \mathrm{d}\Gamma - \int_{\Gamma_\Theta} V \left(\mathbf{\Lambda}^{\mathbf{N}}\right)_{11} \left(6 \cdot \frac{\widehat{\Theta} - \Theta(\boldsymbol{\xi}_{2d})}{2d} - 4 \overline{\nabla}_{\mathbf{N}} \Theta(\boldsymbol{\xi}_d) - \overline{\nabla}_{\mathbf{N}} \Theta(\boldsymbol{\xi}_{2d}) \right) \mathrm{d}\Gamma$$
$$- \int_{\Gamma_\Theta} V \left(\left(\mathbf{\Lambda}^{\mathbf{N}}\right)_{12} \nabla_{\boldsymbol{\xi}} \Theta \cdot \mathbf{S} + \left(\mathbf{\Lambda}^{\mathbf{N}}\right)_{13} \nabla_{\boldsymbol{\xi}} \Theta \cdot \mathbf{R} \right) \mathrm{d}\Gamma + \int_{\Omega} \left(\nabla_{\boldsymbol{\xi}} V\right)^{\mathrm{T}} \mathbf{\Lambda} \nabla_{\boldsymbol{\xi}} \Theta \, \mathrm{d}\Omega$$
$$- \int_{\Gamma_s} [\![V]\!] \left(\mathbf{\Lambda}^{\mathbf{N}}\right)_{11} \left(\frac{3}{2} \cdot \frac{[\![\Theta]\!]_d}{2d} - \frac{1}{2} \cdot \left\langle \nabla_{\boldsymbol{\xi}} \Theta \right\rangle_d \cdot \mathbf{N} \right) \mathrm{d}\Gamma$$
$$- \int_{\Gamma_s} [\![V]\!] \left(\left(\mathbf{\Lambda}^{\mathbf{N}}\right)_{12} \left\langle \nabla_{\boldsymbol{\xi}} \right\rangle \Theta \cdot \mathbf{S} + \left(\mathbf{\Lambda}^{\mathbf{N}}\right)_{13} \left\langle \nabla_{\boldsymbol{\xi}} \right\rangle \Theta \cdot \mathbf{R} \right) \mathrm{d}\Gamma - \int_{\Omega} V R J_F \, \mathrm{d}\Omega = 0. \tag{36}$$

It is convenient to present Eq. (36) using bilinear and linear forms:

$$A(V, \Theta) = P(V), \tag{37}$$

where

$$A(V,\Theta) = \int_{\Gamma_\Theta} V\left(\mathbf{\Lambda^N}\right)_{11}\left(6\cdot\frac{\Theta(\boldsymbol{\xi}_{2d})}{2d} + 4\overline{\nabla}_{\mathbf{N}}\Theta(\boldsymbol{\xi}_d) + \overline{\nabla}_{\mathbf{N}}\Theta(\boldsymbol{\xi}_{2d})\right)\mathrm{d}\Gamma$$
$$- \int_{\Gamma_\Theta} V\left(\left(\mathbf{\Lambda^N}\right)_{12}\nabla_{\boldsymbol{\xi}}\Theta\cdot\mathbf{S} + \left(\mathbf{\Lambda^N}\right)_{13}\nabla_{\boldsymbol{\xi}}\Theta\cdot\mathbf{R}\right)\mathrm{d}\Gamma + \int_{\Omega}\left(\nabla_{\boldsymbol{\xi}}V\right)^{\mathrm{T}}\mathbf{\Lambda}\nabla_{\boldsymbol{\xi}}\Theta\,\mathrm{d}\Omega$$
$$- \int_{\Gamma_s}[\![V]\!]\left(\mathbf{\Lambda^N}\right)_{11}\left(\frac{3}{2}\cdot\frac{[\![\Theta]\!]_d}{2d} - \frac{1}{2}\cdot\left\langle\nabla_{\boldsymbol{\xi}}\Theta\right\rangle_d\cdot\mathbf{N}\right)\mathrm{d}\Gamma$$
$$- \int_{\Gamma_s}[\![V]\!]\left(\left(\mathbf{\Lambda^N}\right)_{12}\left\langle\nabla_{\boldsymbol{\xi}}\right\rangle\Theta\cdot\mathbf{S} + \left(\mathbf{\Lambda^N}\right)_{13}\left\langle\nabla_{\boldsymbol{\xi}}\right\rangle\Theta\cdot\mathbf{R}\right)\mathrm{d}\Gamma, \tag{38}$$

$$P(V) = \int_{\Omega} VRJ_F\,\mathrm{d}\Omega - \int_{\Gamma_q} V\,\widehat{H}J_F^n(\mathbf{n})\,\mathrm{d}\Gamma + 6\int_{\Gamma_\Theta} V\left(\mathbf{\Lambda^N}\right)_{11}\cdot\frac{\widehat{\Theta}}{2d}\,\mathrm{d}\Gamma. \tag{39}$$

3. Approximation

As previously stated, the DGFD method is applied to the reference domain. It means that the discretization, approximation and all calculations are performed for the reference domain Ω. The reference domain is discretized with polyhedral (in 3D) or polygonal (in 2D) mesh. After discretization, Ω is covered by a set of non-overlapping finite elements Ω^e

$$\Omega = \bigcup_e \Omega^e. \tag{40}$$

The approximation in the e-th single finite element is obtained using local basis functions and local degrees of freedom

$$\Theta^e(\boldsymbol{\xi}) = \sum_{i=1}^{n_e} b_i^e(\boldsymbol{\xi})\,\check{\Theta}_i^e = \mathbf{b}^e\,\check{\mathbf{\Theta}}^e, \qquad \text{for } \boldsymbol{\xi}\in\Omega^e, \tag{41}$$

where $\mathbf{b}^e$ is the vector of local basis functions and $\check{\mathbf{\Theta}}^e$ is the vector of local degrees of freedom. The 'local degrees of freedom' indicate degrees of freedom connected with a single finite element and 'local basis functions' mean that the basis functions are defined in the local coordinates connected with the element and their support is limited to the element.

The choice of the local basis functions for each cell is quite arbitrary and depends on the considered problem. However, the polynomial basis functions are widely used since they generally provide correct results for a wide class of problems. During the research associated with this work, various types of basis functions have been tested. Nevertheless, in the presented examples polynomials are used.

In Eq. (41), the approximation for one element cell is shown. It can be rewritten as an approximation for the whole domain

$$\Theta = \mathbf{\Phi}\check{\mathbf{\Theta}}, \qquad \text{for } \boldsymbol{\xi}\in\Omega, \tag{42}$$

where

$$\mathbf{\Phi} = \begin{bmatrix} s^1\mathbf{b}^1 & s^2\mathbf{b}^2 & \dots & s^{Ne}\mathbf{b}^{Ne}\end{bmatrix}, \qquad \check{\mathbf{\Theta}} = \begin{bmatrix}\check{\mathbf{\Theta}}^1\\ \check{\mathbf{\Theta}}^2\\ \vdots\\ \check{\mathbf{\Theta}}^{Ne}\end{bmatrix} \tag{43}$$

and Ne is the number of finite element cells and s^e is the e-th element support, i.e.,

$$s^e = \begin{cases} 1 & \text{for} \quad \boldsymbol{\xi} \in \Omega^e, \\ 0 & \text{for} \quad \boldsymbol{\xi} \notin \Omega^e. \end{cases} \tag{44}$$

The jumps and mid-values are approximated using the same vector of degrees of freedom, i.e.,

$$[\![\Theta]\!] = [\![\boldsymbol{\Phi}]\!]\check{\boldsymbol{\Theta}}, \qquad \langle\Theta\rangle = \langle\boldsymbol{\Phi}\rangle\check{\boldsymbol{\Theta}} \qquad \text{on } \Gamma_s. \tag{45}$$

In the same way, the approximation of the jump and mean values at distance ϵ from Γ_s is defined

$$[\![\Theta]\!]_\epsilon = [\![\boldsymbol{\Phi}]\!]_\epsilon\check{\boldsymbol{\Theta}}, \qquad \langle\Theta\rangle_\epsilon = \langle\boldsymbol{\Phi}\rangle_\epsilon\check{\boldsymbol{\Theta}}. \tag{46}$$

In this paper, the Galerkin formulation is regarded thus, in which the same approximations as in Eqs. (42), (45) and (46) are applied to the test function V.

In this work the polynomial basis functions are obtained from the Taylor series expansion. Each polynomial is defined in e-th cell using local coordinates. In 2D case, the local coordinates (x^e, y^e) are defined in the following way:

$$\xi^e = \frac{\xi - \xi^e_m}{h^e_\xi}, \qquad \eta^e = \frac{\eta - \eta^e_m}{h^e_\eta}, \tag{47}$$

where the point (ξ^e_m, η^e_m) is a center of gravity of the e-th element cell and h^e_ξ, h^e_η are the characteristic lengths of the e-th cell in the x and y directions, respectively. The vectors of basis functions of various degrees of p, which are used in this paper, are as follows:

$$\begin{aligned}
&\text{for } p=1\text{:} \quad \mathbf{b}^e = \mathbf{b}^e_1 = \begin{bmatrix} 1 & \xi^e & \eta^e \end{bmatrix}, \\
&\text{for } p=2\text{:} \quad \mathbf{b}^e = \mathbf{b}^e_2 = \begin{bmatrix} \mathbf{b}^e_1 & \xi^e\eta^e & \xi^{e2} & \eta^{e2} \end{bmatrix}, \\
&\text{for } p=3\text{:} \quad \mathbf{b}^e = \mathbf{b}^e_3 = \begin{bmatrix} \mathbf{b}^e_2 & \xi^{e3} & \xi^{e2}\eta^e & \xi^e\eta^{e2} & \eta^{e3} \end{bmatrix}, \\
&\text{for } p=4\text{:} \quad \mathbf{b}^e = \mathbf{b}^e_4 = \begin{bmatrix} \mathbf{b}^e_3 & \xi^{e4} & \xi^{e3}\eta^e & \xi^{e2}\eta^{e2} & \xi^e\eta^{e3} & \eta^{e4} \end{bmatrix}, \\
&\text{and so on ...}
\end{aligned} \tag{48}$$

When the approximations from Eqs. (42), (45) and (46) are substituted into the weak form Eq. (37), the following linear system of equations is obtained:

$$\boldsymbol{K}\check{\boldsymbol{\Theta}} = \boldsymbol{F}, \tag{49}$$

where

$$\begin{aligned}
\boldsymbol{K} = &\int_\Omega \mathbf{B}^{\mathrm{T}}\boldsymbol{\Lambda}\mathbf{B}\,\mathrm{d}\Omega - \frac{3}{4}\int_{\Gamma_s} \frac{\left(\boldsymbol{\Lambda}^{\mathbf{N}}\right)_{11}}{d}[\![\boldsymbol{\Phi}]\!]^{\mathrm{T}}[\![\boldsymbol{\Phi}]\!]_d\,\mathrm{d}\Gamma + \frac{1}{2}\int_{\Gamma_s}\left(\boldsymbol{\Lambda}^{\mathbf{N}}\right)_{11}[\![\boldsymbol{\Phi}]\!]^{\mathrm{T}}\mathbf{N}^{\mathrm{T}}\langle\mathbf{B}\rangle_d\,\mathrm{d}\Gamma \\
&- \int_{\Gamma_s}\left(\boldsymbol{\Lambda}^{\mathbf{N}}\right)_{12}[\![\boldsymbol{\Phi}]\!]^{\mathrm{T}}\mathbf{S}^{\mathrm{T}}\langle\mathbf{B}\rangle\,\mathrm{d}\Gamma - \int_{\Gamma_s}\left(\boldsymbol{\Lambda}^{\mathbf{N}}\right)_{13}[\![\boldsymbol{\Phi}]\!]^{\mathrm{T}}\mathbf{R}^{\mathrm{T}}\langle\mathbf{B}\rangle\,\mathrm{d}\Gamma \\
&+ 3\int_{\Gamma_\Theta}\frac{\left(\boldsymbol{\Lambda}^{\mathbf{N}}\right)_{11}}{d}\boldsymbol{\Phi}^{\mathrm{T}}\boldsymbol{\Phi}(\boldsymbol{\xi}_{2d})\,\mathrm{d}\Gamma + 4\int_{\Gamma_\Theta}\left(\boldsymbol{\Lambda}^{\mathbf{N}}\right)_{11}\boldsymbol{\Phi}^{\mathrm{T}}\mathbf{N}^{\mathrm{T}}\mathbf{B}(\boldsymbol{\xi}_d)\,\mathrm{d}\Gamma \\
&+ \int_{\Gamma_\Theta}\left(\boldsymbol{\Lambda}^{\mathbf{N}}\right)_{11}\boldsymbol{\Phi}^{\mathrm{T}}\mathbf{N}^{\mathrm{T}}\mathbf{B}(\boldsymbol{\xi}_{2d})\,\mathrm{d}\Gamma - \int_{\Gamma_\Theta}\left(\boldsymbol{\Lambda}^{\mathbf{N}}\right)_{12}\boldsymbol{\Phi}^{\mathrm{T}}\mathbf{S}^{\mathrm{T}}\mathbf{B}\,\mathrm{d}\Gamma - \int_{\Gamma_\Theta}\left(\boldsymbol{\Lambda}^{\mathbf{N}}\right)_{13}\boldsymbol{\Phi}^{\mathrm{T}}\mathbf{R}^{\mathrm{T}}\mathbf{B}\,\mathrm{d}\Gamma,
\end{aligned} \tag{50}$$

$$\boldsymbol{F} = \int_\Omega \boldsymbol{\Phi}^{\mathrm{T}}RJ_F\,\mathrm{d}\Omega - \int_{\Gamma_q}\boldsymbol{\Phi}^{\mathrm{T}}\widehat{H}J^n_F(\mathbf{n})\,\mathrm{d}\Gamma + 3\int_{\Gamma_\Theta}\frac{\left(\boldsymbol{\Lambda}^{\mathbf{N}}\right)_{11}}{d}\boldsymbol{\Phi}^{\mathrm{T}}\widehat{\Theta}\,\mathrm{d}\Gamma$$

and where $\mathbf{B} = \nabla_{\boldsymbol{\xi}}\boldsymbol{\Phi}$.

4. Domain transformation

The method presented in this paper is based on the transformation $\mathbf{x} = \mathbf{x}(\boldsymbol{\xi})$ which has to be known prior to the analysis. The shape of the real domain results from the considered problem, while the shape of the reference domain should be chosen to be as simple as possible. Afterwards, the transformation between these two domains has to be adjusted. In this paper, such a transformation is constructed for each coefficient as a linear combination of a set of basis functions. The parameters of the linear combinations are found by numerical solution of second-order partial differential equations.

In order to describe the transformation between the real domain V and the reference domain Ω the points $\mathbf{x}$ and $\boldsymbol{\xi}$ belonging to the same domains are regarded. Additionally, a set of points $\widehat{\mathbf{x}}$ and $\widehat{\boldsymbol{\xi}}$ is considered, which belongs to the outer boundaries in these domains, i.e.,

$$\begin{aligned} &\mathbf{x} \in V, \qquad \widehat{\mathbf{x}} \in S, \\ &\boldsymbol{\xi} \in \Omega, \qquad \widehat{\boldsymbol{\xi}} \in \Gamma. \end{aligned} \tag{51}$$

For the sake of clarity, the coordinates of the point $\mathbf{x}$ are additionally defined by index

$$\mathbf{x} = \begin{bmatrix} x \\ y \\ z \end{bmatrix} = \begin{bmatrix} x_1 \\ x_2 \\ x_3 \end{bmatrix}. \tag{52}$$

The problem that has to be solved is as follows: find point $\mathbf{x} \in V$ that is the projection of point $\boldsymbol{\xi} \in \Omega$ and $\widehat{\mathbf{x}} = \widehat{\mathbf{x}}(\widehat{\boldsymbol{\xi}})$. There is no unique solution of the problem, since there are no possible transformations. However, we want to find a transformation that is smooth and can be expressed as a linear combination of a set of basis functions. This can be obtained by numerical solution of a series of differential boundary problems defined for each coefficient of point $\mathbf{x}$, i.e.,

$$\begin{aligned} &\nabla_{\boldsymbol{\xi}}^{\mathrm{T}} \left(\nabla_{\boldsymbol{\xi}} x_i \right) = 0 \qquad \text{on } \Omega \\ &x_i = \widehat{x_i} \qquad\qquad\ \ \text{on } \Gamma \end{aligned} \qquad \text{for } i = 1, 2, 3, \tag{53}$$

where $\widehat{x_i} = \widehat{x_i}(\widehat{\boldsymbol{\xi}})$ is the transformation of the outer boundary in the reference configuration Γ into the outer boundary in the real boundary S for the i-th coefficient. This transformation is incorporated into the problem in Eq. (53).

The weak form of the problem presented in Eq. (53) with a test function W is

$$-\int_{\Omega} \nabla_{\boldsymbol{\xi}} W^{\mathrm{T}} \nabla_{\boldsymbol{\xi}} x_i \, \mathrm{d}\Omega + \int_{\Gamma} W \mathbf{N}^{\mathrm{T}} \nabla_{\boldsymbol{\xi}} \, x_i \, \mathrm{d}\Gamma = 0 \qquad \forall \, W \qquad \text{for } i = 1, 2, 3. \tag{54}$$

The Dirichlet boundary conditions are applied with the help of fourth-degree finite difference rule, in the same way as in the DGFD method

$$\mathbf{N}^{\mathrm{T}} \nabla_{\boldsymbol{\xi}} \, x_i = 6 \cdot \frac{\widehat{x_i} - x_i(\boldsymbol{\xi}_{2d})}{2d} - 4\mathbf{N}^{\mathrm{T}} \nabla_{\boldsymbol{\xi}} \, x_i(\boldsymbol{\xi}_d) - \mathbf{N}^{\mathrm{T}} \nabla_{\boldsymbol{\xi}} \, x_i(\boldsymbol{\xi}_{2d}). \tag{55}$$

The coefficients x_i are going to be found using a linear combination of basis functions

$$x_i \left(\boldsymbol{\xi} \right) = \mathbf{b} \left(\boldsymbol{\xi} \right) \check{\mathbf{x}}_i = \boldsymbol{\Phi} \check{\mathbf{x}}_i. \tag{56}$$

When Eqs. (55) and (56) are substituted in to a weak form in Eq. (54) the following linear system of equations is obtained:

$$\boldsymbol{M} \check{\mathbf{x}}_i = \boldsymbol{P}_i, \qquad i = 1, 2, 3, \tag{57}$$

where

$$\boldsymbol{M} = \int_{\Omega} \mathbf{B}^{\mathrm{T}}\mathbf{B}\,\mathrm{d}\Omega + \int_{\Gamma} \frac{3}{d}\boldsymbol{\Phi}^{\mathrm{T}}\boldsymbol{\Phi}(\boldsymbol{\xi}_{2d})\,\mathrm{d}\Gamma + 4\int_{\Gamma} \boldsymbol{\Phi}^{\mathrm{T}}\mathbf{N}^{\mathrm{T}}\mathbf{B}(\boldsymbol{\xi}_{d})\,\mathrm{d}\Gamma + \int_{\Gamma} \boldsymbol{\Phi}^{\mathrm{T}}\mathbf{N}^{\mathrm{T}}\mathbf{B}(\boldsymbol{\xi}_{2d})\,\mathrm{d}\Gamma,$$
$$\boldsymbol{P}_i = \int_{\Gamma} \frac{3}{d}\boldsymbol{\Phi}^{\mathrm{T}}\widehat{x}_i\,\mathrm{d}\Gamma. \tag{58}$$

The matrix on the left side of Eq. (56) is the same for each i. There are three different right-side vectors in 3D or two vectors in 2D. The matrix $\boldsymbol{M}$ in Eq. (57) can be factorized just once to find three vectors of degrees of freedom for each of the coefficients.

The numerical illustration of the transformation is presented in Appendix where a quarter of annulus disc is considered.

5. Examples

In this section, the examples that illustrate the calculations in the reference domain are discussed. In order to show the correctness of the approach, a set of benchmark tests is presented. The benchmark tests are based on the following boundary problem:

$$-\Delta\Theta = f(x,y). \tag{59}$$

The boundary conditions and the right-hand side function $f(x,y)$ are derived from the exact solution $\Theta(x,y)$ that is

$$\Theta(x,y) = x^2\,y + \sin(2\,\pi\,x)\sin(2\,\pi\,y) \tag{60}$$

and the right-hand side function is:

$$f(x,y) = 2y - 8\,\pi^2\sin(2\,\pi\,x)\sin(2\,\pi\,y). \tag{61}$$

The exact solution of the problem is depicted in Fig. 2 in the square domain of $[-1,\,1]\times[-1,\,1]$. It can be noticed that the function strongly fluctuates and has large gradients.

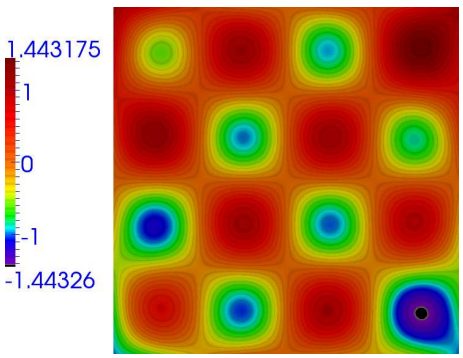

Fig. 2. Exact solution for the considered example in $[-1,\,1]\times[-1,\,1]$ domain.

The problem in Eq. (59) is examined for a set of domains with various shapes. Types of domains are shown in Fig. 3. In the following subsections, all the details concerning the subdomains and the calculation results are discussed.

Each domain considered in this section is transformed into $[-1,\,1]\times[-1,\,1]$ domain. On the reference quadrilateral domain the Dirichlet boundary conditions are set on the left and right sides,

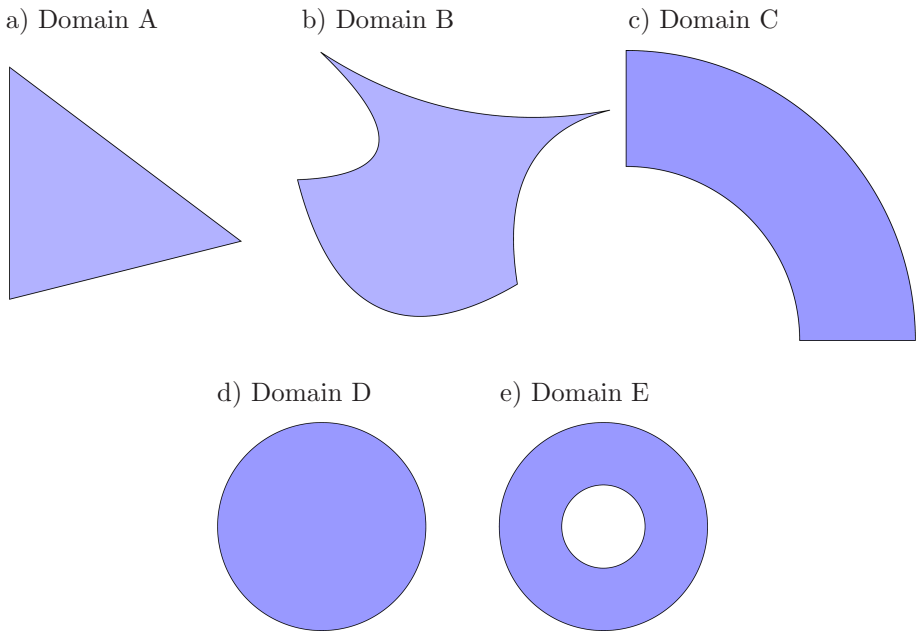

Fig. 3. Three kinds of domains considered in the benchmark tests.

and Neumann boundary conditions are set on the upper and lower sides. The polygonal mesh is generated on the reference domain. For the sake of clarity, the same mesh is used for each of the reference domain. The reference domain with boundary conditions and the mesh are presented in Fig. 4. The Dirichlet boundary conditions $\widehat{\Theta}$ and the heat flux for the Neumann boundary conditions $\widehat{H}$ are taken from the exact solution of problem (59).

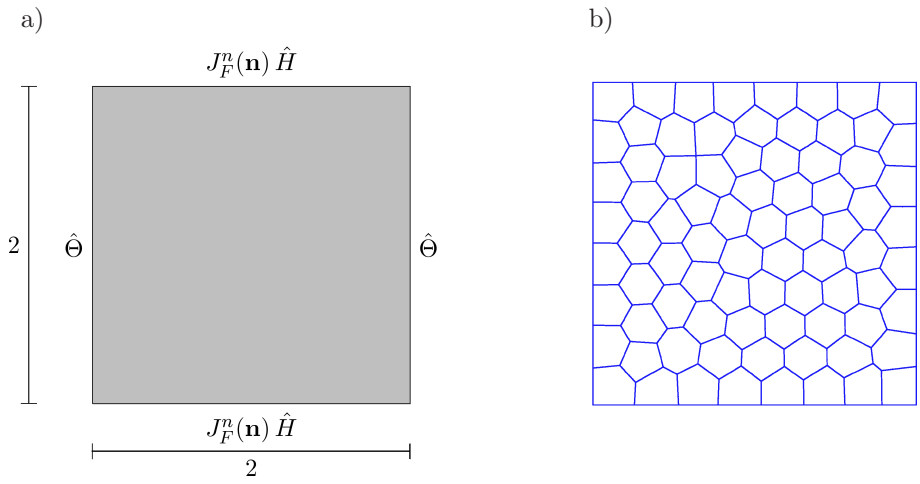

Fig. 4. a) Reference domain with Dirichlet and Neumann boundary conditions, b) the polygonal mesh in the $[-1, 1] \times [-1, 1]$ reference domain (80 cells).

The mesh consists of 80 polygonal cells. In each cell seventh-degree polynomial approximation is applied (36 basis functions). The number of degrees is 2880 in each case.

In the discussed examples, the error of the approximate solutions is measured. The definition of the error at an arbitrary point in V is defined as

$$e = \left|\Theta - \overline{\Theta}\right| \qquad \text{in } V, \tag{62}$$

where e is the error of the approximate solution, Θ is the exact solution, and $\overline{\Theta}$ is the approximate solution. In order to measure the global error of the approximate solution the L_2 norm and H_1 semi-norm are used, which are respectively defined as follows

$$\begin{aligned} \|e\|_{L_2} &= \sqrt{\int_V \left(\Theta - \overline{\Theta}\right)^2 \mathrm{d}V}, \\ |e|_{H_1} &= \sqrt{\int_V \left(\nabla\Theta - \nabla\overline{\Theta}\right)^{\mathrm{T}} \left(\nabla\Theta - \nabla\overline{\Theta}\right) \mathrm{d}V}. \end{aligned} \tag{63}$$

5.1. Domain A

In this section, a domain of triangular shape is considered. In order to show the correctness of the presented approach the domain shown in Fig. 5 is in fact quadrangle, but one of its sides is very short ($2 \cdot 10^{-6}$ times smaller in comparison to other sides).

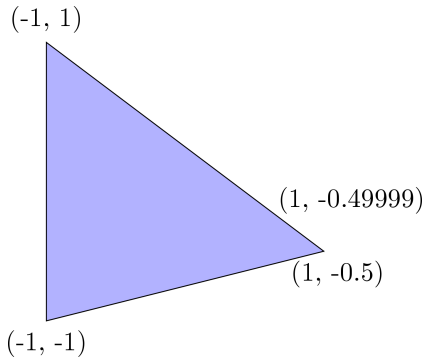

Fig. 5. Domain A.

The transformations for the considered domain are

$$\begin{aligned} x &= \xi, \\ y &= -0.25 - 0.25\,\xi + 0.5\,\eta - 0.5\,\xi\,\eta. \end{aligned} \tag{64}$$

The results are presented in Fig. 6 where the approximate solution in reference and real domain are shown and the error distribution in the real domain proves the correctness of the method.

In the example, the right side has been extended $2 \cdot 10^6$ times in the transformation to the square reference domain. At the same time, the left side is not extended at all. In spite of such a level of extension between the real and reference domains the obtained approximate solution is quite accurate. It indicates that in a case of great 'deformations' the calculations are not disturbed, and even the error is not concentrated in the place with great 'deformation'.

For comparison, the same problem was additionally solved by the DGFD method on the real domain. It means that Domain A was discretized by finite element mesh, Fig. 7a, which also consists of 80 polygonal cells. Also, in this case the seventh-degree polynomial approximation is applied to each cell. The approximate solution in this case is also very close to the exact solution and the error distribution of the approximate solution is presented in Fig. 7b. It can be noticed that the errors for the results obtained on the reference domain, Fig. 6d, are on similar level as those obtained on real domain, Fig. 7b. However, in the case of Fig. 6d the errors are concentrated close to upper vertex and in the case of results in Fig. 7b the error is uniformly distributed in the domain.

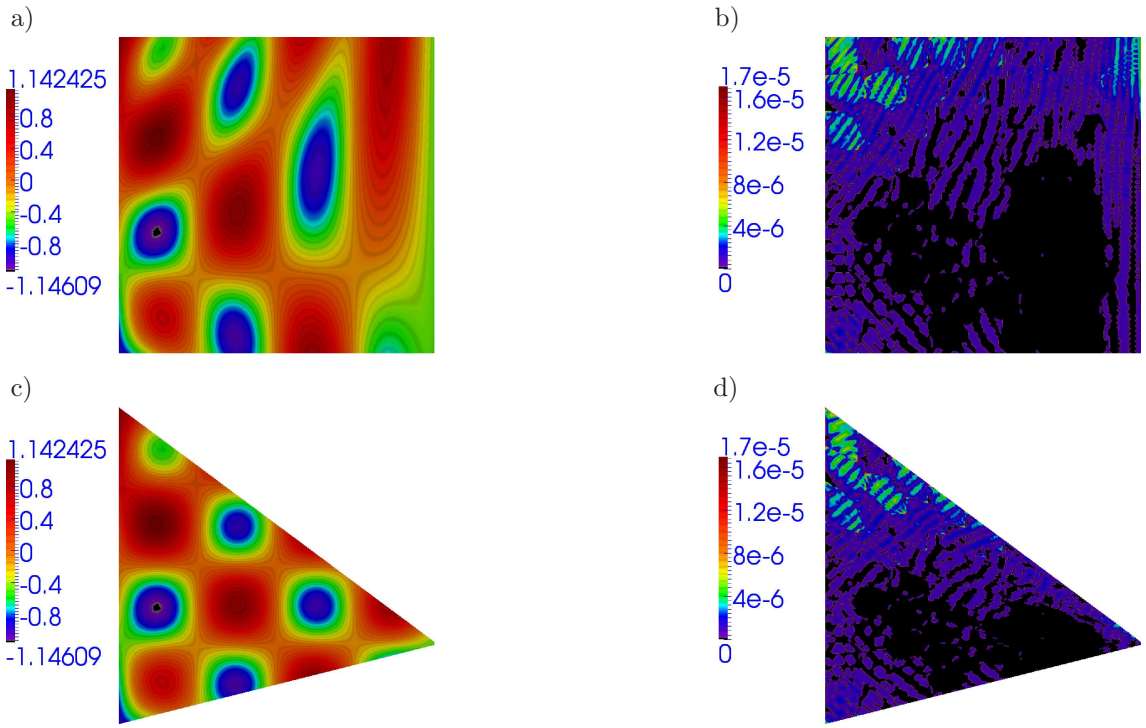

Fig. 6. Results for Domain A: a) approximate solution in reference domain, b) solution error in reference domain, c) approximate solution in real domain, d) solution error in real domain.

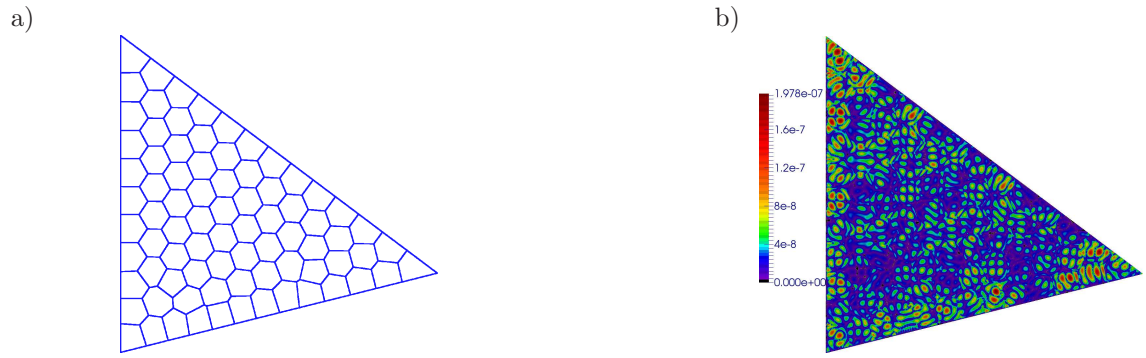

Fig. 7. Mesh and solution error for Domain A obtained on the real domain: a) mesh on the real domain with 80 cells, b) solution error obtained in real domain.

5.2. Domain B

This time, a domain of a quite arbitrary shape presented in Fig. 8 is considered. It can be seen that the left side is strongly concave and the lower side is convex, in opposite. At two upper vertices the domain constricts so that the domain is very thin there.

The transformations from the reference domain to the real one, in this case, are as follows:

$$\begin{aligned} x &= 0 + 0.65\,\xi + 0.35\,\eta + 0.15\,\xi\eta + 0.15\,\xi^2 - 0.15\,\eta^2 - 0.1\,\xi^2\eta + 0.45\,\xi\eta^2, \\ y &= -0.35 - 0.1\,\xi + 0.85\,\eta + 0.1\,\xi\eta + 0.45\,\xi^2 + 0\,\eta^2 - 0.2\,\xi^2\eta - 0.25\,\xi\eta^2. \end{aligned} \tag{65}$$

Once again the problem from Eq. (59) has been solved on the reference domain with the transformations described in Eq. (65). The results of the calculations are presented in Fig. 9 including the approximate solution on the reference and real domains and the error distribution in the real domain.

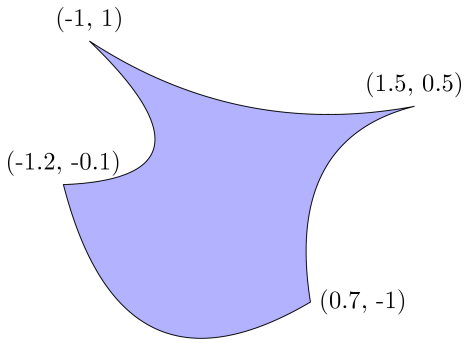

Fig. 8. Domain B with vertices coordinates.

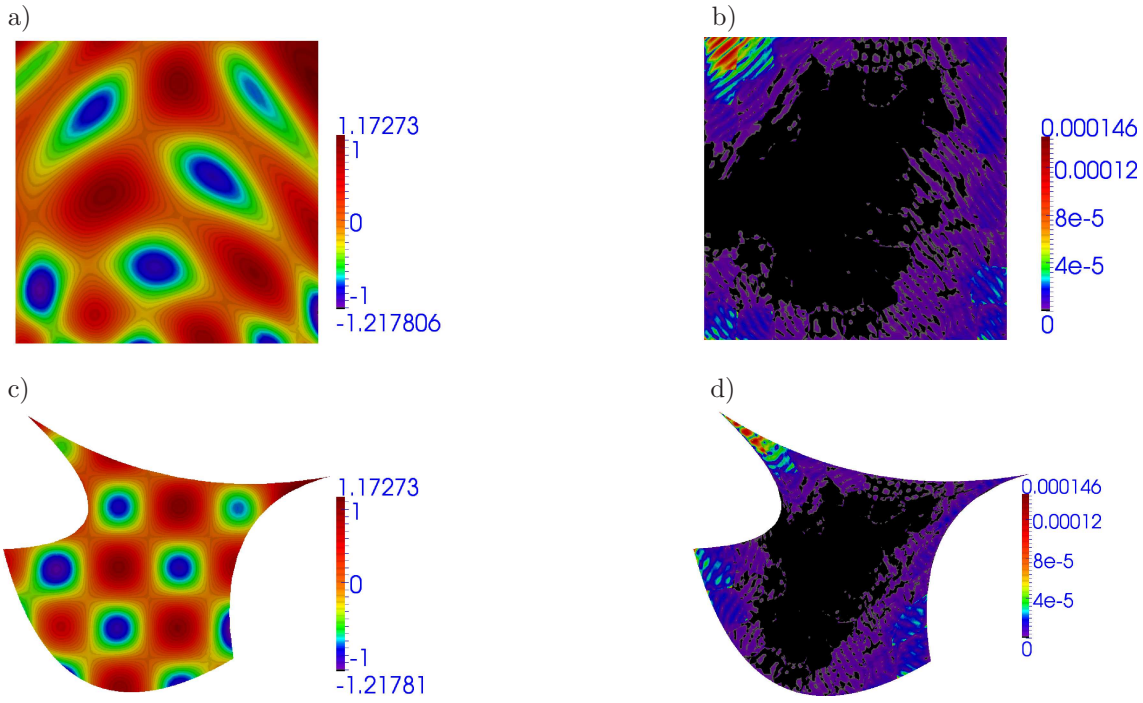

Fig. 9. Results for Domain B: a) approximate solution in reference domain, b) solution error in reference domain, c) approximate solution in real domain, d) solution error in real domain.

In spite of the fact that Domain B has a very thin part and one of its sides is strongly concave, the obtained results are quite satisfactory. The error is concentrated on the left upper corner with the level of $1 \cdot 10^{-4}$. However, in the rest of the domain the error is lower than $1 \cdot 10^{-5}$.

5.3. Domain C

In this section, a domain that has a shape of quarter of annulus is examined, see Fig. 10. The domain is defined by the outer R and inner r radii. The transformation from the square reference domain to the real one is described in details in Appendix. In this example, three versions of the domain are studied in which $r = 1, 1.8, 1.98$ and $R = 2$ for each case. In the situation when $r = 1.98$ the domain is very thin, but this fact does not cause any changes in the presented algorithm. It can be noticed that the algorithm can cope with wide variety of domains with quite arbitrary shapes.

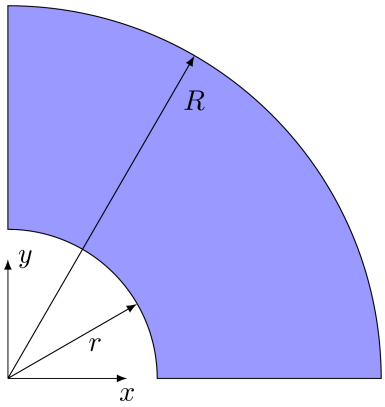

Fig. 10. Domain C with inner and outer radius.

Each of the three cases requires transformations from the square reference domain into the real one. The transformations are as follows:

1. The transformations for the first case, $R = 2$ and $r = 1$, are as follows:

$$\begin{aligned} x &= 1.635\eta + 0.25555\xi\eta - 0.104\xi^2\eta - 0.1281\eta^3 \\ &\quad + 1.0607\sin\left(\frac{\pi}{4}\xi\right) + 1.0607\cos\left(\frac{\pi}{4}\xi\right) - 1.6318\sin\left(\frac{\pi}{4}\eta\right), \\ y &= 1.635\eta - 0.25555\xi\eta - 0.104\xi^2\eta - 0.1281\eta^3 \\ &\quad - 1.0607\sin\left(\frac{\pi}{4}\xi\right) + 1.0607\cos\left(\frac{\pi}{4}\xi\right) - 1.6318\sin\left(\frac{\pi}{4}\eta\right). \end{aligned} \tag{66}$$

2. In the second case, the transformations for $R = 2$ and $r = 1.8$ are

$$\begin{aligned} x &= 0.327\eta + 0.0511\xi\eta - 0.0208\xi^2\eta - 0.0256\eta^3 \\ &\quad + 1.3435\sin\left(\frac{\pi}{4}\xi\right) + 1.3435\cos\left(\frac{\pi}{4}\xi\right) - 0.3264\sin\left(\frac{\pi}{4}\eta\right), \\ y &= 0.327\eta - 0.0511\xi\eta - 0.0208\xi^2\eta - 0.0256\eta^3 \\ &\quad - 1.3435\sin\left(\frac{\pi}{4}\xi\right) + 1.3435\cos\left(\frac{\pi}{4}\xi\right) - 0.3264\sin\left(\frac{\pi}{4}\eta\right). \end{aligned} \tag{67}$$

3. The last, third case is for with $R = 2$ and $r = 1.98$ and the transformations are expressed as

$$\begin{aligned} x &= 0.0327\eta + 0.00511\xi\eta - 0.00208\xi^2\eta - 0.00256\eta^3 \\ &\quad + 1.4071\sin\left(\frac{\pi}{4}\xi\right) + 1.4071\cos\left(\frac{\pi}{4}\xi\right) - 0.03264\sin\left(\frac{\pi}{4}\eta\right), \\ y &= 0.0327\eta - 0.00511\xi\eta - 0.00208\xi^2\eta - 0.00256\eta^3 \\ &\quad - 1.4071\sin\left(\frac{\pi}{4}\xi\right) + 1.4071\cos\left(\frac{\pi}{4}\xi\right) - 0.03264\sin\left(\frac{\pi}{4}\eta\right). \end{aligned} \tag{68}$$

The results for the three cases are presented in Figs. 11–13, where the approximate solution and the error map on the reference and real domains are shown. The results in each case are

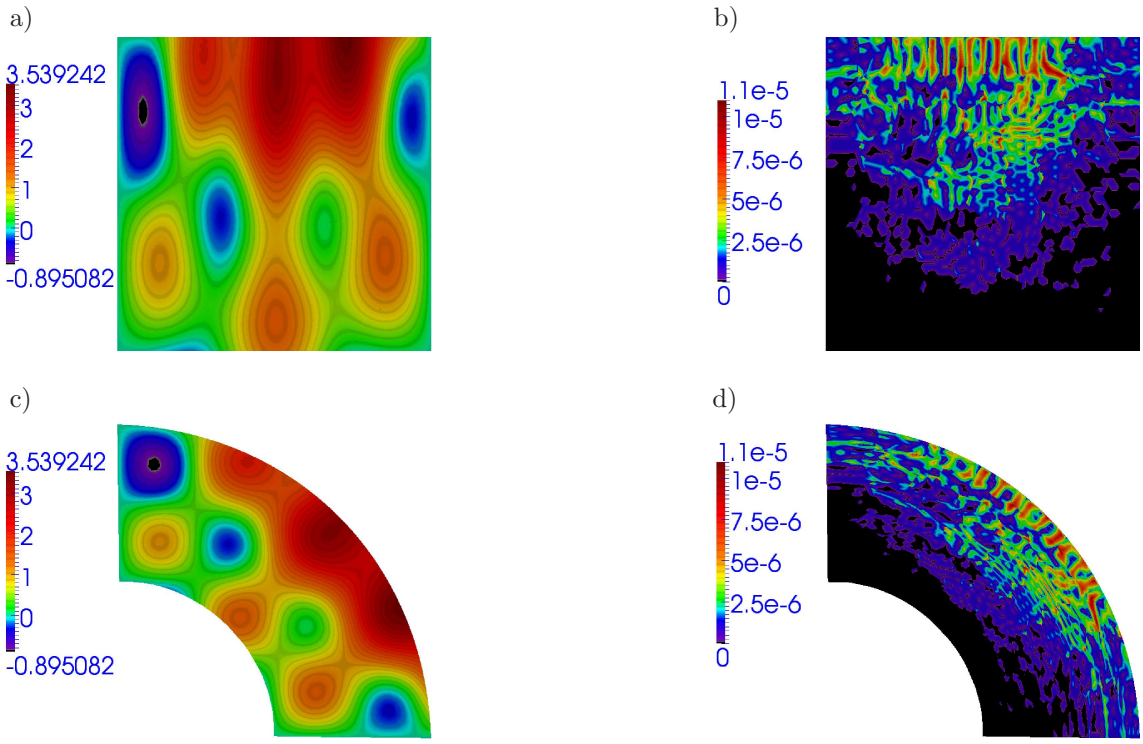

Fig. 11. Results for Domain C, $R = 2$ and $r = 1$: a) approximate solution in reference domain, b) solution error in reference domain, c) approximate solution in real domain, d) solution error in real domain.

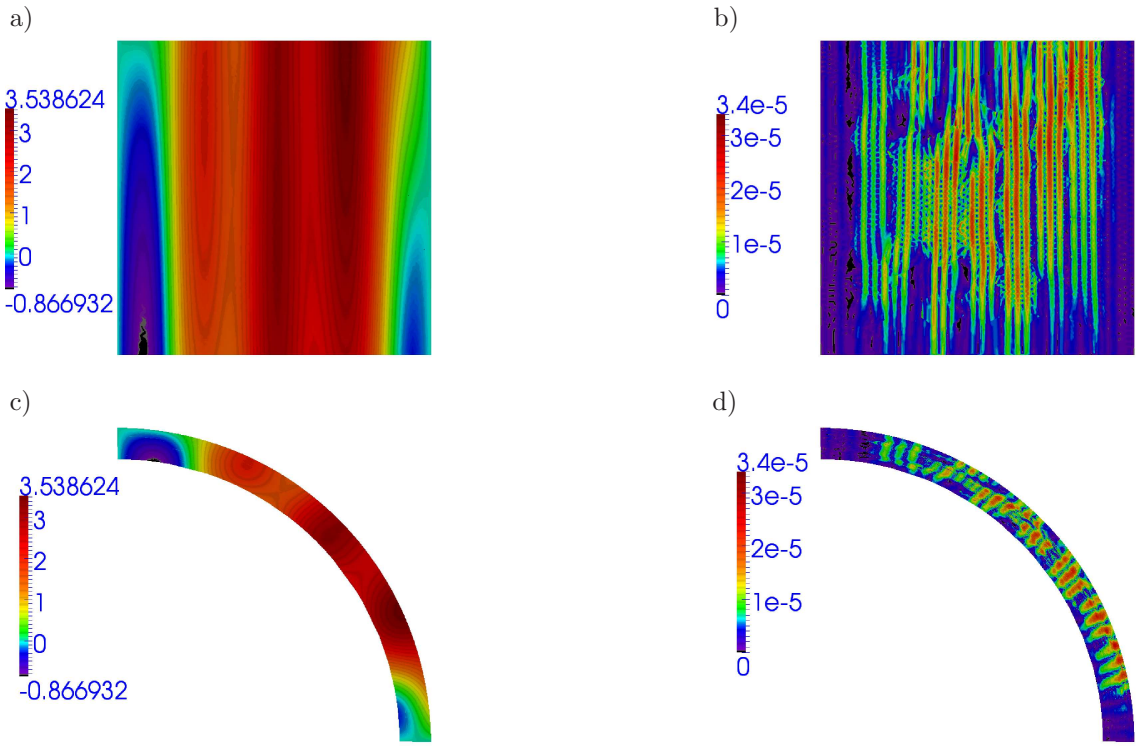

Fig. 12. Results for Domain C, $R = 2$ and $r = 1.8$: a) approximate solution in reference domain, b) solution error in reference domain, c) approximate solution in real domain, d) solution error in real domain.

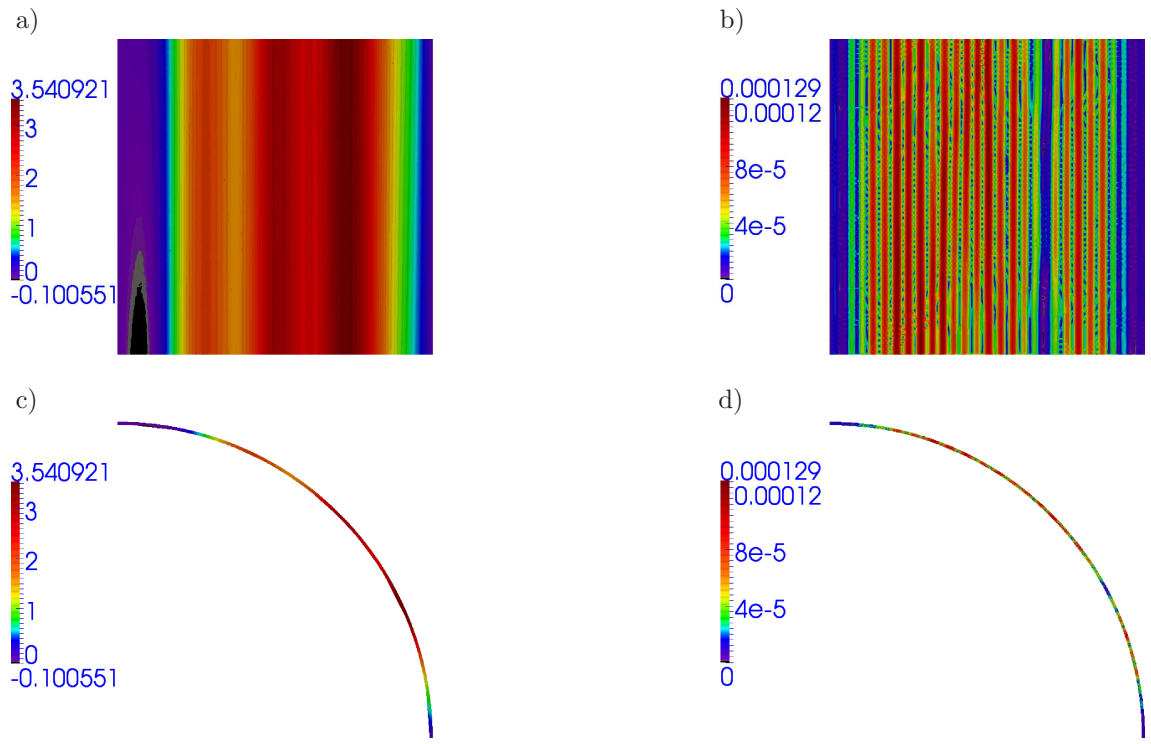

Fig. 13. Results for Domain C, $R = 2$ and $r = 1.98$: a) approximate solution in reference domain, b) solution error in reference domain, c) approximate solution in real domain, d) solution error in real domain.

satisfactorily good. However, it can be noticed that in the third case the error level is much higher in comparison to the two other cases, see Figs. 11b, 12b and 13b. It can be concluded that in the last case the domain is strongly 'squeezed' after the transformations. In this case, the domain width is 0.02 and is transformed from the reference domain of size 2.

It seems that in the last case, another reference domain should be chosen to reduce the discrepancy between the dimensions of reference and real domain. Therefore, the longitudinal rectangular reference domain with the polygonal mesh of 80 finite elements is considered, see Fig. 14. All three cases of Domain C are recalculated on the rectangular reference domain. The results can be then easily compared with those obtained on the square reference domain. Thereby, it is also shown that the algorithm derived in this paper is independent of the choice of the reference domain.

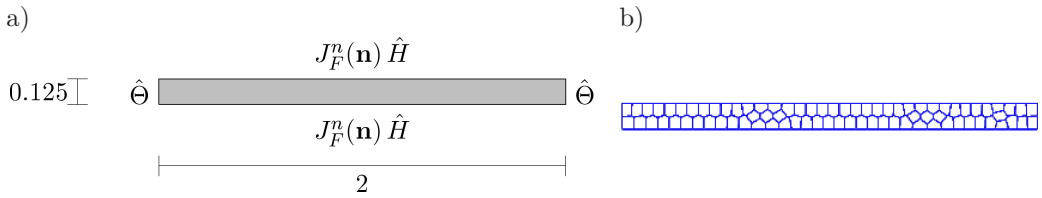

Fig. 14. a) Rectangular reference domain with Dirichlet and Neumann boundary conditions, b) polygonal mesh in the $[-0.0625, 0.0625] \times [-1, 1]$ reference domain (80 cells).

The transformations from the reference domain to the real domains are calculated using the algorithm described in Sec. 4 and also in this case the trigonometric basis functions are used. For the sake of the paper's clarity these transformations are not included. The same seventh-degree approximation is used for finite elements, as for the square reference domain. The results of the calculations are presented in Figs. 15–17.

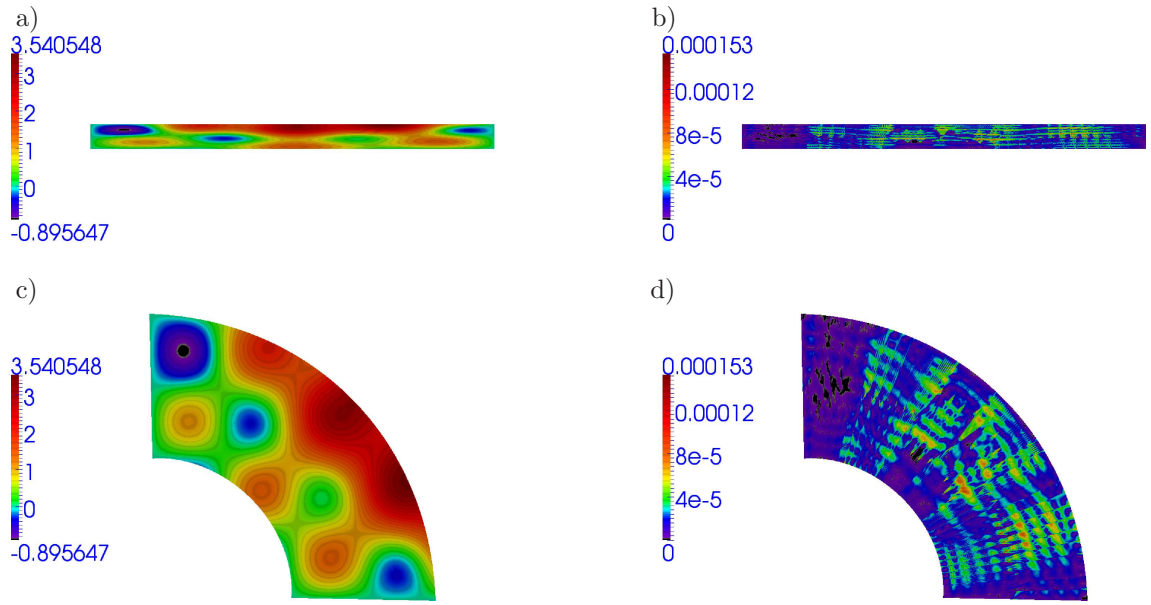

Fig. 15. Results for Domain C, $R = 2$ and $r = 1$, and rectangular reference domain: a) approximate solution in reference domain, b) solution error in reference domain, c) approximate solution in real domain, d) solution error in real domain.

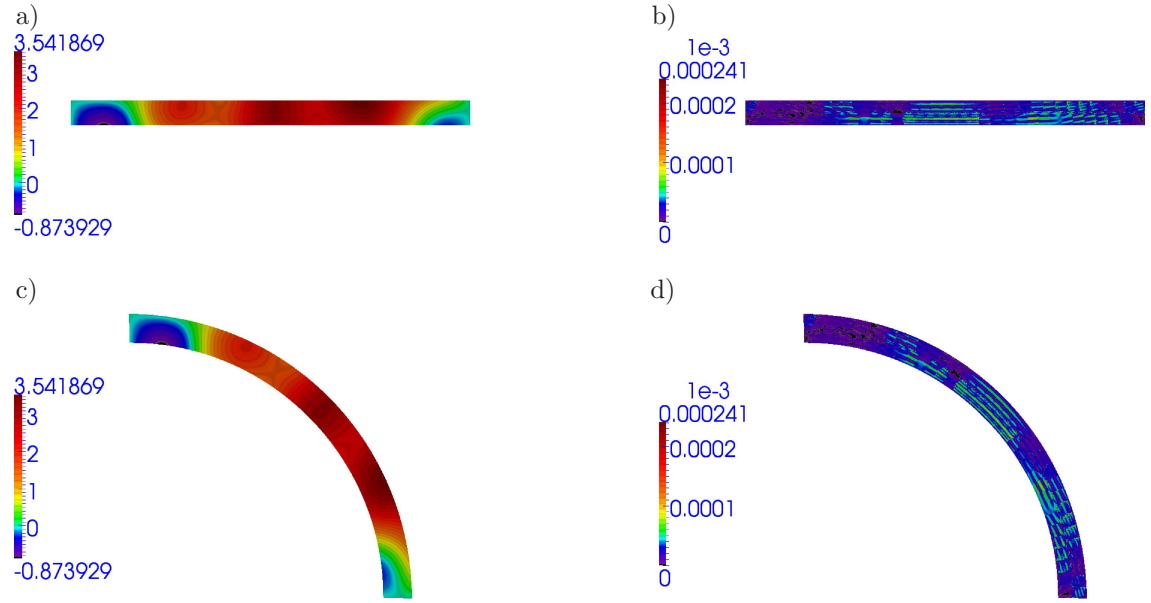

Fig. 16. Results for Domain C, $R = 2$ and $r = 1.8$, and rectangular reference domain: a) approximate solution in reference domain, b) solution error in reference domain, c) approximate solution in real domain, d) solution error in real domain.

It can be seen that all the results calculated on the rectangular domain are correct. However, for the first case ($r = 1$) the results are slightly worse in comparison to the square domain. However, in two other cases ($r = 1.8$ and $r = 1.98$) the error levels are much lower now. It can be concluded here that, in spite of the fact that the presented algorithm works in general arbitrary reference domain, better results can be obtained if the shape of the reference domain matches that of the real one. Thereby, the transformation does not generate large gradients that may lead to severe numerical truncation errors.

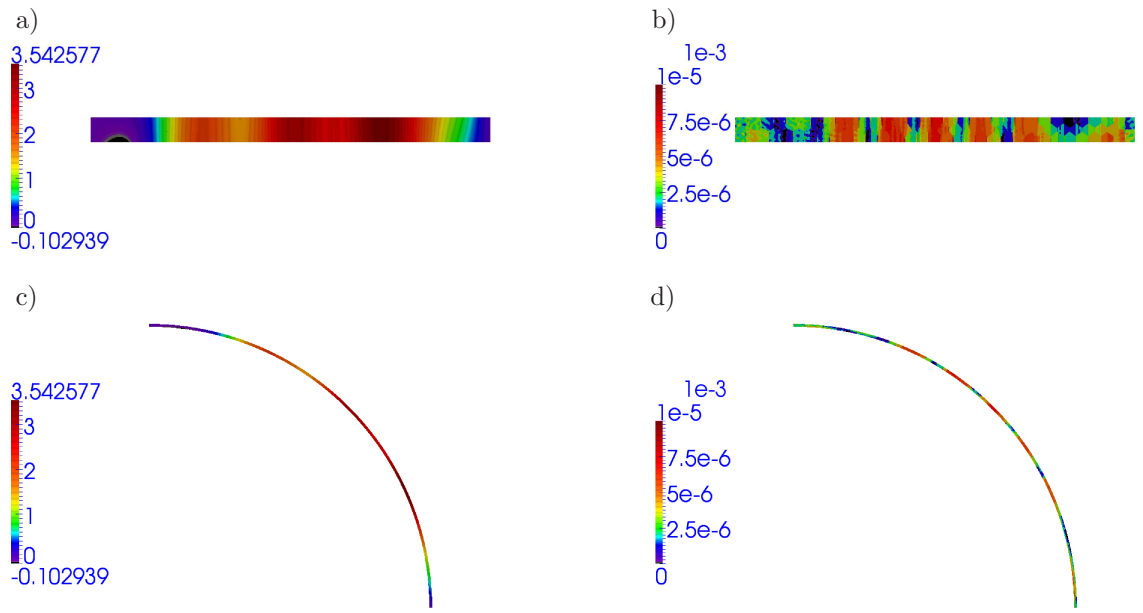

Fig. 17. Results for Domain C, $R = 2$ and $r = 1.98$, and rectangular reference domain: a) approximate solution in reference domain, b) solution error in reference domain, c) approximate solution in real domain, d) solution error in real domain.

5.4. Domain D

Now, a circular domain with radius $R = 1$ is regarded. The reference domain is the square domain as shown in Fig. 4. In order to set the outer boundary transformation, the external boundary circle is divided into four equal segments. Then, each side from the reference domain is transformed into the boundary segment in the real domain, as shown in Fig. 18.

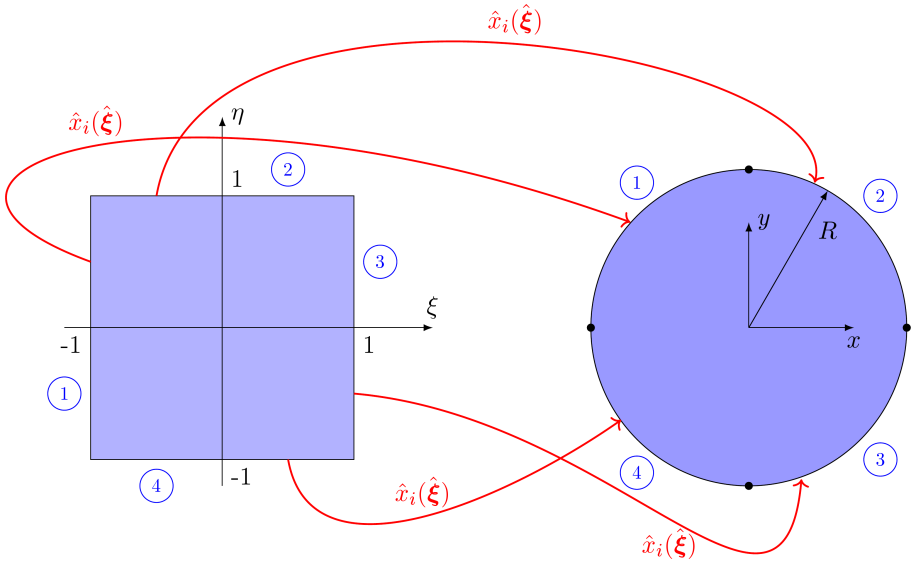

Fig. 18. Transformations of the outer boundary of Domain D with radius $R = 1$.

The transformations of the outer boundary segment from the reference domain to the outer boundary segment in the real domain are as follows:

$$
\begin{aligned}
&1\text{:}\quad \widehat{x} = R\cos\left(\frac{3}{4}\pi - \frac{\widehat{\eta}}{4}\pi\right), \qquad \widehat{y} = R\sin\left(\frac{3}{4}\pi - \frac{\widehat{\eta}}{4}\pi\right),\\
&2\text{:}\quad \widehat{x} = R\cos\left(\frac{1}{4}\pi - \frac{\widehat{\xi}}{4}\pi\right), \qquad \widehat{y} = R\sin\left(\frac{1}{4}\pi - \frac{\widehat{\xi}}{4}\pi\right),\\
&3\text{:}\quad \widehat{x} = R\cos\left(-\frac{1}{4}\pi + \frac{\widehat{\eta}}{4}\pi\right), \qquad \widehat{y} = R\sin\left(-\frac{1}{4}\pi + \frac{\widehat{\eta}}{4}\pi\right),\\
&4\text{:}\quad \widehat{x} = R\cos\left(-\frac{3}{4}\pi + \frac{\widehat{\xi}}{4}\pi\right), \qquad \widehat{y} = R\sin\left(-\frac{3}{4}\pi + \frac{\widehat{\xi}}{4}\pi\right).
\end{aligned}
\tag{69}
$$

Finally, the transformations from the reference into real domain in this case has been calculated as

$$
\begin{aligned}
x = {} & 2.77\xi + 2.77\eta - 0.2562\xi^3 - 0.208\xi^2\eta - 0.208\xi\eta^2 - 0.2562\eta^3 \\
& - 2.5564\sin\left(\frac{\pi}{4}\xi\right) - 2.5564\sin\left(\frac{\pi}{4}\eta\right),\\
y = {} & -2.77\xi + 2.77\eta + 0.2562\xi^3 - 0.208\xi^2\eta + 0.208\xi\eta^2 - 0.2562\eta^3 \\
& + 2.5564\sin\left(\frac{\pi}{4}\xi\right) - 2.5564\sin\left(\frac{\pi}{4}\eta\right).
\end{aligned}
\tag{70}
$$

The results are presented in Fig. 19. Once again the obtained results are quite satisfactory. In spite of the fact that the real domain does not have vertexes, the computations can be done on the square reference domain.

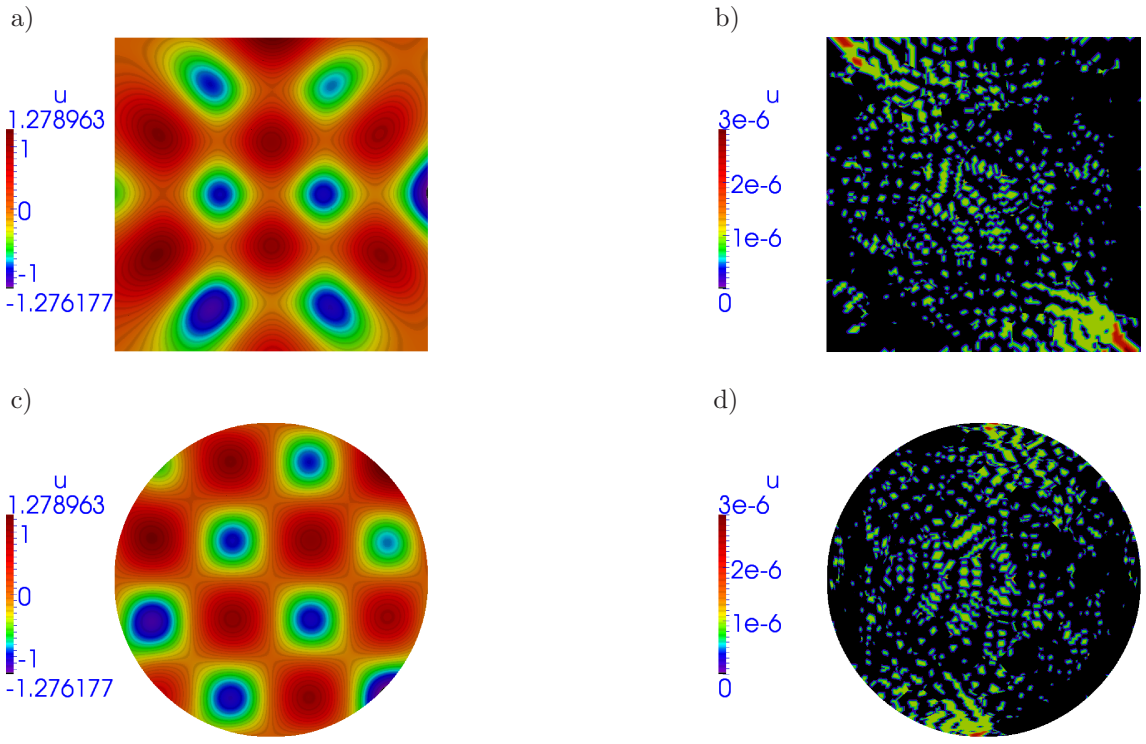

Fig. 19. Results for Domain D: a) approximate solution in reference domain, b) solution error in reference domain, c) approximate solution in real domain, d) solution error in real domain.

5.5. Domain E

In this example, an annulus domain with outer radius $R = 1$ and inner radius $r = 0.4$ is studied. The real domain has a central circular hole; therefore, the reference domain also has to have a hole inside. Thus, the reference domain is a square with a square hole in the middle, as shown in Fig. 20.

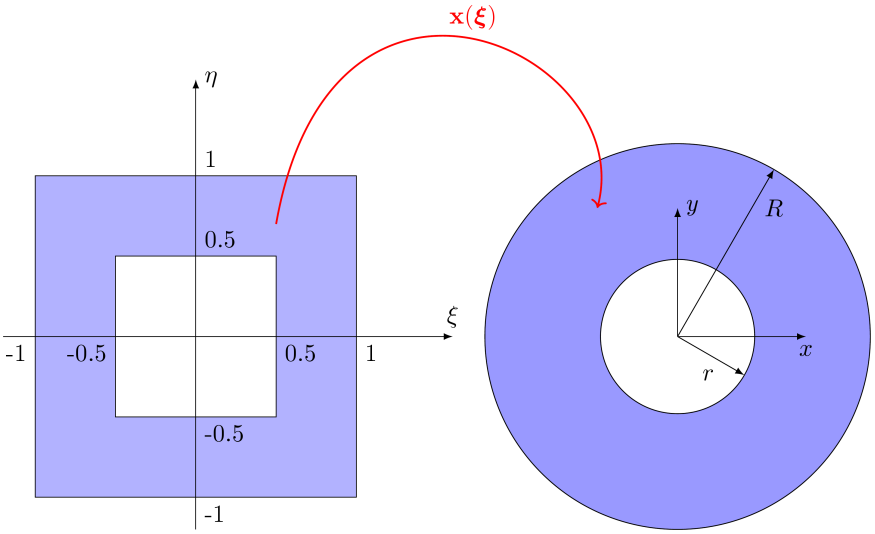

Fig. 20. Transformation of the outer boundary of Domain E with outer radius $R = 1$ and inner radius $r = 0.4$.

In the transformation the outer and inner boundaries have to be considered. In this case, the 10th-degree vector of basis functions is used to obtain the transformation $\mathbf{x}(\boldsymbol{\xi})$. The reference domain has been discretized by three meshes: by a 12th-degree non-simply-connected finite element, Fig. 21a, by four 10th-degree non-simply-connected finite elements, Fig. 21b and by polygonal mesh with 80 elements, Fig. 21c. For details on non-simply-connected finite elements see [12].

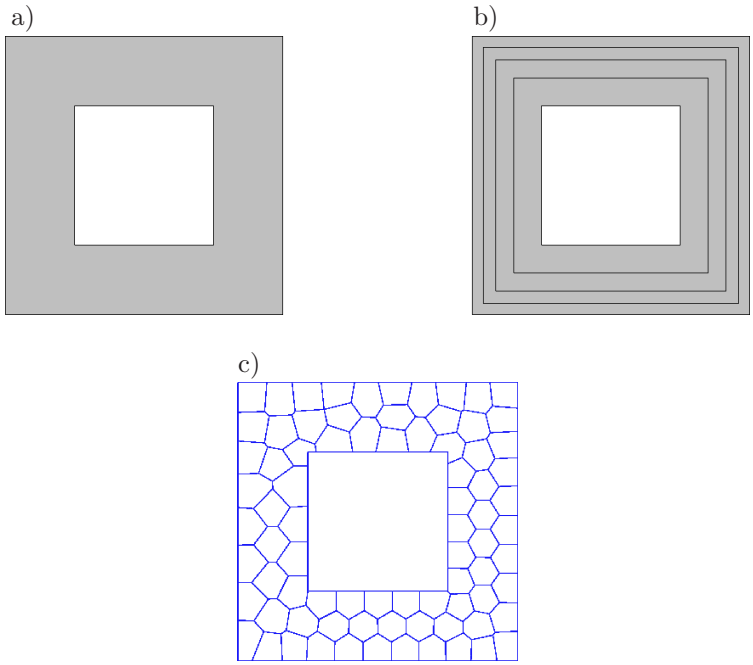

Fig. 21. Three meshes in the reference domain with a hole inside: a) mesh with one non-simply-connected element, b) mesh with four non-simply-connected elements, c) polygonal mesh with 80 elements.

The results for the three meshes are presented in the same manner as in the cases of other examples. Figure 22 shows the results for the one-element mesh (Fig. 21a). The results for the four-element mesh (Fig. 21b) are presented in Fig. 23. Finally, the results for the polygonal mesh

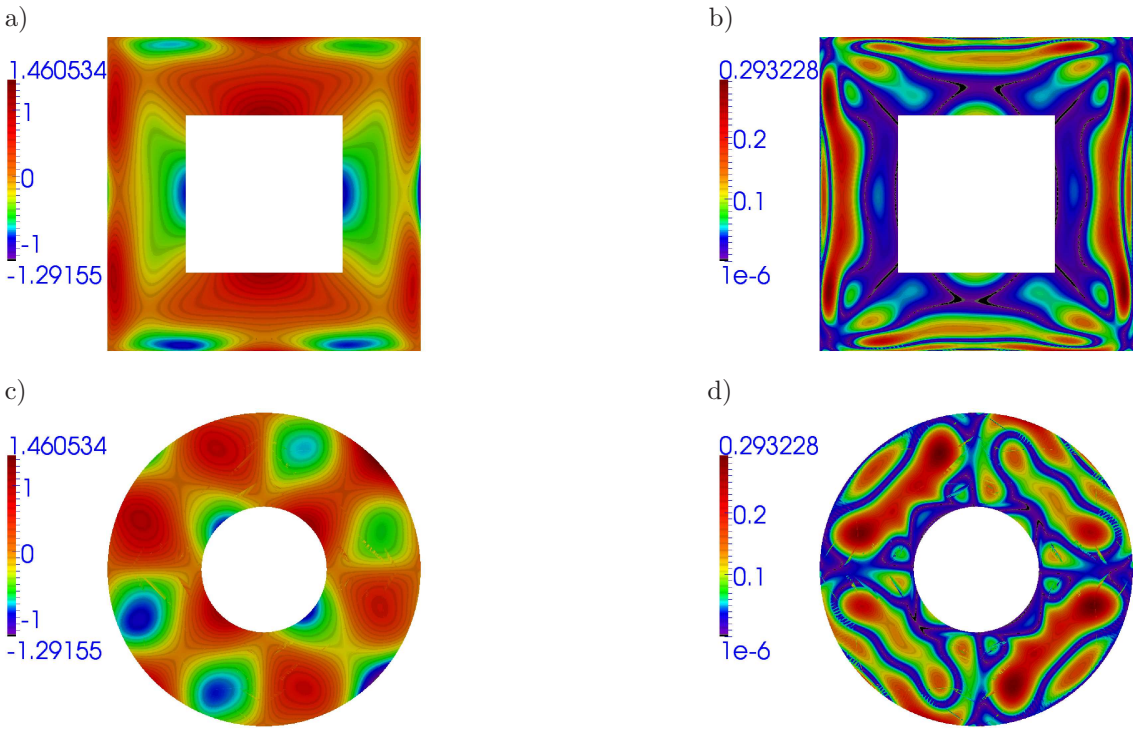

Fig. 22. Results for Domain E for one-element mesh from Fig. 21a and 12th-degree approximation: a) approximate solution in reference domain, b) solution error in reference domain, c) approximate solution in real domain, d) solution error in real domain.

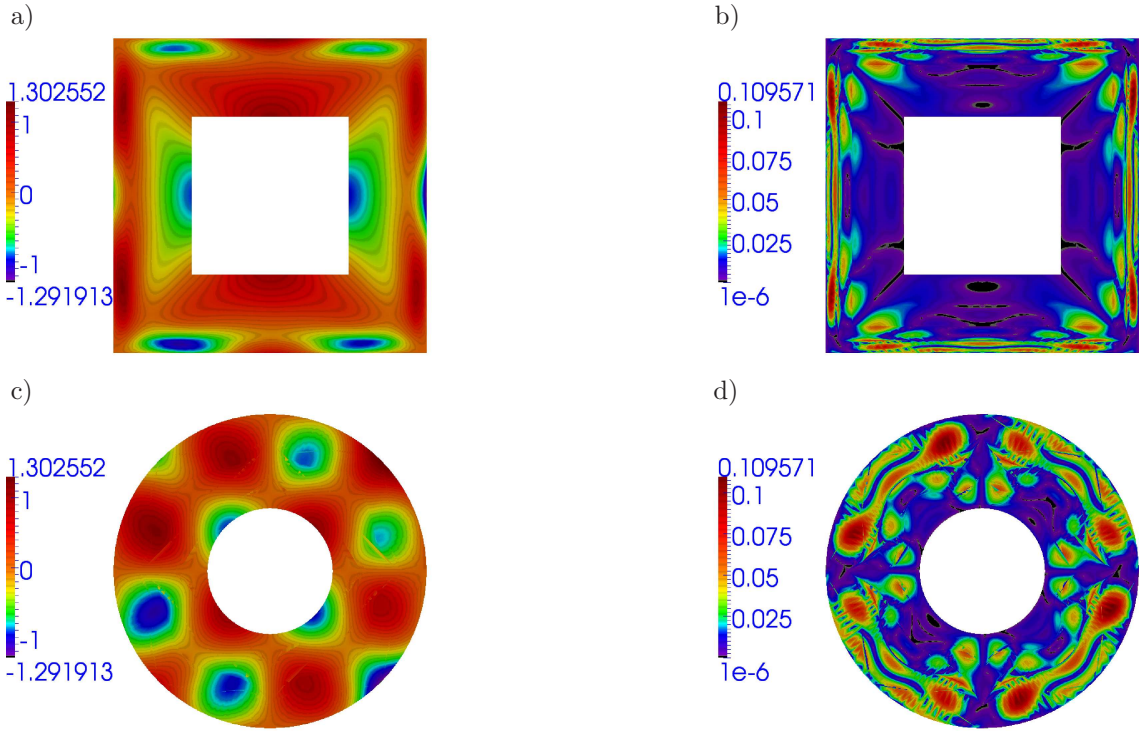

Fig. 23. Results for Domain E for four-element mesh from Fig. 21b and 10th-degree approximation: a) approximate solution in reference domain, b) solution error in reference domain, c) approximate solution in real domain, d) solution error in real domain.

(Fig. 21c) are included in Fig. 24. As can be noticed, the obtained results are quite accurate even for meshes with one or four elements. It is shown, in the example, that the domain with an inside hole can be transformed to an appropriate reference domain.

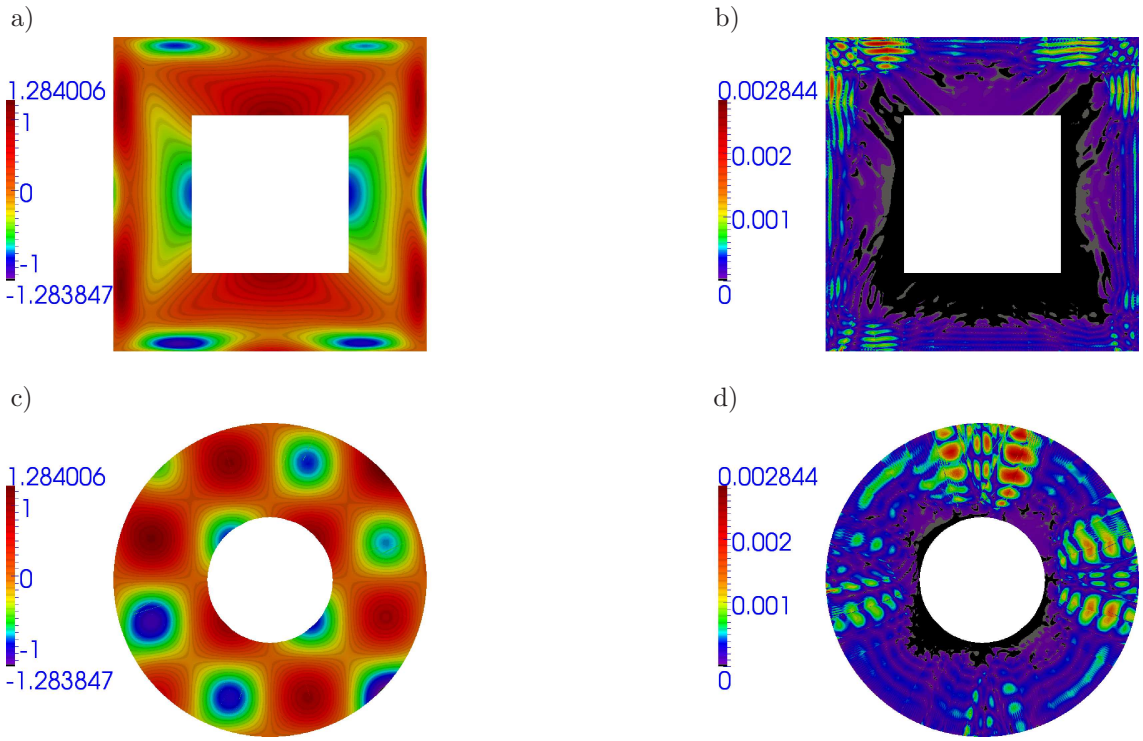

Fig. 24. Results for Domain E for mesh from Fig. 21 and seventh-degree approximation: a) approximate solution in reference domain, b) solution error in reference domain, c) approximate solution in real domain, d) solution error in real domain.

6. Conclusions

The DGFG method on the reference domain has been presented. In the proposed approach, the problem defined on the real domain is numerically analyzed in the reference domain. It is shown in a series of benchmark examples that the proposed approach is correct and effective. In the approach, the considered problem is transformed into the reference domain which has a simple shape and is easy to mesh. The transformation from the reference domain into the real one has to be obtained first, and then the transformation is incorporated into the analysis on the reference domain. Such a procedure helps to cope with domains with complicated shapes and with curved boundaries.

In this work, the method for the transformation generation is proposed. This method is based on the second-order partial differential equation that has to be solved on the reference domain for each coefficient. In order to get domain transformation, first we need to set the outer boundary transformation. On the other hand, on outer boundary of the real domain the boundary conditions are defined which also need to be transformed onto the reference domain. The equations, written in weak forms, are solved using the DGFD method with one element. The special basis functions or high-degree polynomials can be used to obtain the transformation. In the presented examples, the trigonometric function or 10th-degree polynomials are used. As a result, exact geometry is maintained or at least approximated with high accuracy.

As it is shown in the examples, the DGFD method in the reference domain gives a great and new opportunity in solving boundary problems on arbitrary domains. The effects obtained in this work are quite similar to the ones given by isogeometric analysis (IGA). However, no control points

or complicated shape functions are needed. Both the transformation and solution of the boundary problems are constructed on basis functions which can be chosen adequately for the considered problem.

The continuation of this research will concern the three-dimensional analysis and adoption of the description to elasticity and thermo-elasticity problems. The future research will also be focused on the improvement of the transformation technique so that it can cope with three-dimensional complicated domains.

Appendix

The transformation presented in Sec. 4 is illustrated here by the two-dimensional example, in which a square reference domain is transformed into a quarter of annulus. The boundary problem from Eq. (53) requires first a formulation of the boundary conditions. In this case, the outer boundary in the reference domain has to be transformed to the outer boundary in the real domain. The boundaries of Ω and V domains are divided into four segments. Each segment from the reference domain is separately transformed to the boundary segment of the annulus quarter as shown in Fig. A1. The mathematical transformation, written for each of segments, is as follows:

$$
\begin{aligned}
&1\text{:} \quad \widehat{x} = 0, && \widehat{y} = r + \frac{1}{2}(R-r)(\eta+1),\\
&2\text{:} \quad \widehat{x} = R\sin\left(\frac{\pi}{4}+\frac{\pi}{4}\widehat{\xi}\right), && \widehat{y} = R\cos\left(\frac{\pi}{4}+\frac{\pi}{4}\widehat{\xi}\right),\\
&3\text{:} \quad \widehat{x} = R - \frac{1}{2}(R-r)(1-\eta), && \widehat{y} = 0,\\
&4\text{:} \quad \widehat{x} = r\cos\left(\frac{\pi}{4}-\frac{\pi}{4}\widehat{\xi}\right), && \widehat{y} = r\sin\left(\frac{\pi}{4}-\frac{\pi}{4}\widehat{\xi}\right).
\end{aligned}
\tag{A1}
$$

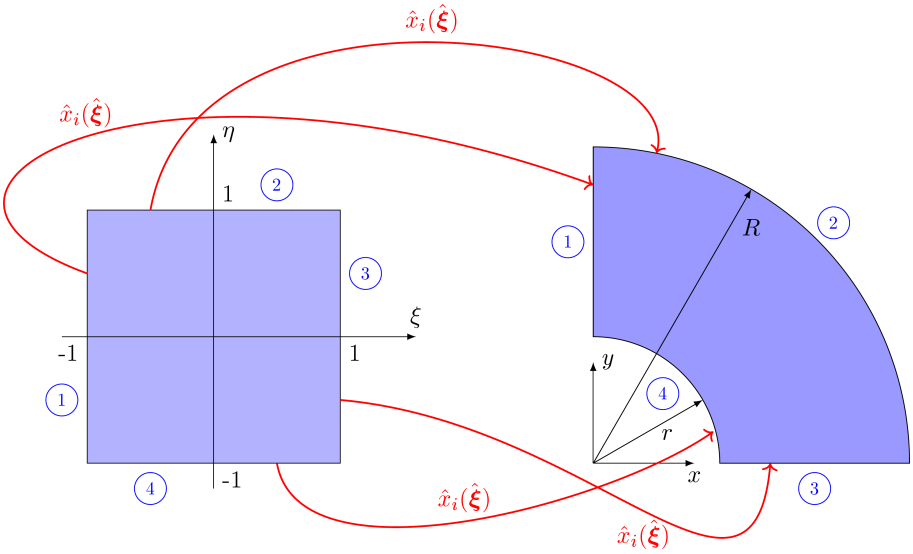

Fig. A1. Illustrative example of the transformation procedure from reference to real domains.

For the considered domain, the set of basis functions for the transformation has been chosen as

$$
\mathbf{b}(\boldsymbol{\xi}) = \left[\mathbf{b}_3(\boldsymbol{\xi}) \quad \sin\left(\frac{\pi}{4}\xi\right) \quad \cos\left(\frac{\pi}{4}\xi\right) \quad \sin\left(\frac{\pi}{4}\eta\right) \quad \cos\left(\frac{\pi}{4}\eta\right)\right], \tag{A2}
$$

where $\mathbf{b}_3$ is the set of polynomial basis functions of third order (10 basis polynomial functions) presented in Eq. (48).

The boundary transformation in Eq. (A1) and the vector of basis functions in Eq. (A2) are applied to the Eq. (57) for both the coefficients, i.e., x and y, and for $R = 2$ and $r = 1$. After solution of these two systems of equations the vectors of degrees of freedom are obtained as

$$\check{\boldsymbol{x}} = \begin{bmatrix} 0 \\ 0 \\ 1.6350 \\ 0.2555 \\ 0 \\ 0 \\ 0 \\ -0.1040 \\ 0 \\ -0.1281 \\ 1.0607 \\ 1.0607 \\ -1.6318 \\ 0 \end{bmatrix}, \qquad \check{\boldsymbol{y}} = \begin{bmatrix} 0 \\ 0 \\ 1.6350 \\ -0.2555 \\ 0 \\ 0 \\ 0 \\ -0.1040 \\ 0 \\ -0.1281 \\ -1.0607 \\ 1.0607 \\ -1.6318 \\ 0 \end{bmatrix}. \tag{A3}$$

References

[1] A. Bartezzaghi, L. Dedè, A. Quarteroni. Isogeometric analysis of high order partial differential equations on surfaces. *Computer Methods in Applied Mechanics and Engineering*, **295**: 446–469, 2015.

[2] B.B. Cockburn, G. Karniadakis, C.-W. Shu [Eds.]. *Discontinuous Galerkin methods: theory, computation, and applications*. Lecture notes in Computational Science and Engineering. Springer, Berlin, New York, 2000.

[3] J.A. Cottrell, T.J.R. Hughes, Y. Bazilevs. *Isogeometric analysis: toward integration of CAD and FEA*. Wiley, 2009.

[4] D.A. Di Pietro, A. Ern. *Mathematical aspects of discontinuous Galerkin methods*. Mathématiques et Applications. Springer Berlin Heidelberg, 2011.

[5] J. Donea, S. Giuliani, J.P. Halleux. An arbitrary Lagrangian-Eulerian finite element method for transient dynamic fluid-structure interactions. *Computer Methods in Applied Mechanics and Engineering*, **33**(1): 689–723, 1982.

[6] J. Donea, A. Huerta, J.-Ph. Ponthot, A. Rodríguez-Ferran. *Arbitrary Lagrangian-Eulerian methods*. John Wiley & Sons, Ltd, 2004.

[7] R.M. Franck, R.B. Lazarus. *Mixed Eulerian-Lagrangian method*, Vol. 3, pp. 47–67. Academic Press Inc.: New York, 1964.

[8] J.S. Hesthaven, T. Warburton. *Nodal discontinuous Galerkin methods: algorithms, analysis, and applications*. Springer Publishing Company, Incorporated, 1st Edition, 2007.

[9] C.W. Hirt, A.A. Amsden, J.L. Cook. An arbitrary Lagrangian-Eulerian computing method for all flow speeds. *Journal of Computational Physics*, **14**(3): 227–253, 1974.

[10] T.J.R. Hughes, J.A. Cottrell, Y. Bazilevs. Isogeometric analysis: CAD, finite elements, NURBS, exact geometry and mesh refinement. *Computer Methods in Applied Mechanics and Engineering*, **194**(39–41): 4135–4195, 2005.

[11] J. Jaśkowiec. The discontinuous Galerkin method with higher degree finite difference compatibility conditions and arbitrary local and global basis functions. *Computer Assisted Methods in Engineering and Science*, in print.

[12] J. Jaśkowiec, P. Pluciński, A. Stankiewicz. Discontinuous Galerkin method with arbitrary polygonal finite elements. *Finite Elements in Analysis and Design*, in print.

[13] I. Lomtev, R.M. Kirby, G.E. Karniadakis. A discontinuous Galerkin ALE method for compressible viscous flows in moving domains. *Journal of Computational Physics*, **155**(1): 128–159, 1999.

[14] V.-T. Nguyen. An arbitrary Lagrangian-Eulerian discontinuous Galerkin method for simulations of flows over variable geometries. *Journal of Fluids and Structures*, **26**(2): 312–329, 2010.

[15] L. Noels, R. Radovitzky. A new discontinuous Galerkin method for non-linear mechanics. In *47th AIAA/ASME/ASCE/AHS/ASC Structures, Structural Dynamics, and Materials Conference*, Newport, Rhode Island, May 2006. American Institute of Aeronautics and Astronautics.

[16] J. Tinsley Oden. A short-course on nonlinear continuum mechanics. CAM 397, Introduction to Mathematical Modeling, Third Edition, 2008.
[17] P.-O. Persson, J. Bonet, J. Peraire. Discontinuous Galerkin solution of the Navier-Stokes equations on deformable domains. *Computer Methods in Applied Mechanics and Engineering*, **198**(17–20): 1585–1595, 2009.
[18] W.H. Reed, T.R. Hill. *Triangular mesh methods for the neutron transport equation*. In: National Topical Meeting on Mathematical Models and Computational Techniques for Analysis of Nuclear Systems, Ann Arbor, Michigan, USA, 8 Apr 1973.
[19] B. Rivière. *Discontinuous Galerkin methods for solving elliptic and parabolic equations*. Society for Industrial and Applied Mathematics, 2008.
[20] L. Wang, P.-O. Persson. A high-order discontinuous Galerkin method with unstructured space-time meshes for two-dimensional compressible flows on domains with large deformations. *Computers & Fluids*, **118**: 53–68, 2015.